Mobile gamma spectrometry: Development and optimisation of methods for locating and mapping lost radioactive sources

Nilsson, Jonas

2016

Document Version:
Förlagets slutgiltiga version

Mobile Gamma Spectrometry

Development and Optimisation of Methods for Locating and Mapping Lost Radioactive Sources

JONAS NILSSON

LUND UNIVERSITY

Doctoral Thesis
2016

Medical Radiation Physics, Malmö
Lund University, Sweden

Faculty opponent
Professor David C.W. Sanderson, University of Glasgow, Scotland

ISSN 1652–8220 • ISBN 978–91–7619–317–4

The public defense of this thesis for the degree Doctor of Philosophy in Medical Radiation Physics will, with due permission from the Faculty of Medicine at Lund University, take place in Room 2005-2007, Inga-Marie Nilssons gata 49, Malmö, on Friday, 9 September 2016, at 09.00.

Cover:
The figure illustrates the mathematical response function of a detector passing a radioactive source as well as simulations of this. Each diamond represent an event registered by the detector and the number in each simulation plot is the maximum number of events registered within an integration time of fixed length.

Typeset using LaTeX and the template *SE-PhDThesis*, adapted from work by Erik Hedström and available at: `https://github.com/SkyToGround/SE-PhDThesis`.

Printed by: MEDIA-TRYCK, Lund, Sweden

mjc.nilsson@gmail.com

ISSN 1652–8220
ISBN 978–91–7619–317–4
Medical Radiation Physics, Malmö, Lund University
SE-221 00 LUND, Sweden

– Unfinished experiments

– Unwritten text

– Time you do not have

Things which are useless to a PhD student

Contents

List of original papers

This thesis is based on the following papers, which in the text will be referred to by their Roman numerals.

I. **A deviation display method for visualising data in mobile gamma-ray spectrometry** Kock P., Finck R.R., Nilsson J.M.C., Östlund K. and Samuelsson C. *Applied Radiation and Isotopes* 2010 68(9); pp 1832-1838

II. **Tests of HPGe- and scintillation-based backpack γ-radiation survey systems** Nilsson J.M.C., Östlund K., Söderberg J., Mattsson S. and Rääf C. *Journal of Environmental Radioactivity* 2014 135; pp 54-62

III. **Investigation and optimisation of mobile NaI(Tl) and ^{3}He-based neutron detectors for finding point sources** Nilsson J.M.C., Finck R.R. and Rääf C. *Nuclear Instruments & Methods in Physics Research A* 2015 786; pp 127-134

IV. **A rotating-slit-collimator-based gamma radiation mapper** Nilsson J.M.C., Finck R.R. and Rääf C. Manuscript submitted to *Journal of Environmental Radioactivity*

V. **Sensitivity of mobile gamma spectrometry systems to point sources** Nilsson J.M.C., Finck R.R. and Rääf C. Manuscript submitted to *Nuclear Instruments & Methods in Physics Research A*

Abstract

This thesis describes methods and detector systems developed to improve the probability of detecting radioactive sources out of regulatory control, orphaned sources, as well as methods for determining the location of these sources. Mobile spectrometry systems, light enough to be carried in a backpack, were compared by applying statistics to data collected using these systems in laboratory experiments as well as field tests. The results from these tests can be used to determine which detector system to use when surveying ares for radioactive sources on foot. New visualisation methods and analysis methods were also developed to improve the sensitivity of the backpack systems, as well as other mobile gamma spectrometry systems, to radioactive sources.

By modifying a gamma spectrometer intended for airborne and carborne use, a neutron radiation detector was created. Its sensitivity was compared to that of a dedicated neutron detector, with favourably results, using mathematical models to simulate mobile measurements. The mathematical models were also extended and generalised in order to determine optimal measurement parameters of mobile gamma spectrometry systems. These models indicated that gains in sensitivity could be found by optimising the measurement parameters to a given measurement scenario.

A system was built that can be used to create maps of radiation fields in an area. The system is based on a directional gamma spectrometry system which is used to scan the area of interest from several locations around the area. The resulting data is processed in order to improve the angular resolution. This data is in turn fed to an image reconstruction algorithm that creates the map. The system was tested by scanning an area containing three radioactive sources and the results from the image reconstruction, correctly indicated the locations of the sources.

Populärvetenskaplig sammanfattning

Radioaktiva strålkällor som inte hanteras eller förvaras av en organisation som har tillstånd för att använda dessa kan betraktas som borttappade eller herrelösa strålkällor. Då dessa strålkällor utsänder joniserande strålning som i vissa fall kan vara farlig för allmänheten så ligger det i samhällets intresse att det bedrivs forskning på metoder och mätutrustning som kan användas till att hitta och omhänderta strålkällor av detta slag. De fem vetenskapliga arbeten som presenteras här har haft som mål att förbättra sannolikheten för att hitta borttappade strålkällor genom förbättring av existerande mätmetoder samt utveckling av nya mätsystem.

Gammastrålning är en typ av joniserande strålning som utsänds av många radioaktiva strålkällor varför detektorer som kan registrera denna typ av strålning oftast används vid sökning av radioaktiva strålkällor. När strålningen träffar detektorn så omvandlas den till en elektrisk signal som kan registreras av en dator. Den elektriska signalen har också en signatur som kan användas för att identifiera vilken typ av radioaktiv strålkälla som den joniserande strålningen ursprungligen kom ifrån.

I det första forskningsprojektet som presenteras i avhandlingen så beskrivs beräkningar som använder signaturen i den elektriska signalen till att skapa bilder av strålningen som detektorn registrerar. Dessa bilder visar strålningen på ett sätt som gör det lättare att avgöra om det verkligen finns en borttappad strålkälla i närheten eller om det bara är naturligt förekommande bakgrundsstrålning som detektorn registrerar. I det efterföljande arbetat så undersöktes fler sätt att skapa bilder och kartor av den joniserande strålningen för att göra det lättare för den som mäter strålningen att avgöra om det finns borttappade strålkällor i närheten. I detta arbete undersöktes också tre olika typer av detektorer för att ta reda på vilken som passar bäst när större områden ska genom-

sökas till fots. Som en vidareutveckling av detta så presenteras också matematik som kan användas för att beräkna (och därmed också maximera) sannolikheten för att en detektor ska detektera en borttappad strålkälla.

Neutronstrålning är en typ av joniserande strålning som kan vara svår att detektera direkt men denna typ av strålning producerar också gammastrålning som en bieffekt. Genom att modifiera detektorer avsedda för att mäta gammastrålning så kan de indirekt detektera neutronstrålning och detta undersöktes i ett av forskningsprojekten. I ett annat av de forskningsprojekt som nämns i avhandlingen så utvecklades det en detektor som är riktningskänslig. Genom att göra beräkningar på den strålning som denna detektor registrerar så går inte bara att göra bilder som visar om det finns borttappade strålkällor i närheten, utan också bilder som säger var strålkällan är placerad.

Trots att strålningsdetektorer har använts relativt länge för att hitta borttappade och herrelösa strålkällor så visar de arbeten som presenteras här att det fortfarande finns mycket forskning som kan bedrivas på ämnet. Genom att använda välkända statistiska modeller och fysikaliska fenomen så kan känsligheten i existerande mätsystem ökas. Metoder och matematik som används inom andra forskningsområden kan också anpassas för att förbättra existerande och skapa nya typer av mätsystem inom mobil gammaspektrometri.

Abbreviations

Technical terms

FWHM	Full Width at Half Maximum
HPGe	High-Purity Germanium
$LaBr_3$:Ce	Lanthanum Bromide doped with Cerium
NaI(Tl)	Sodium Iodide doped with Thallium
PSF	Point Spread Function
ROI	Region Of Interest

Organisations

IAEA	International Atomic Energy Agency
SSM	Swedish Radiation Safety Authority

Chapter 1

Introduction

1.1 Historical background

The history of what we today call ionising radiation can be said to have started with the discovery of X-rays by Wilhelm Röntgen in 1895. This was quickly followed by the discovery of radiation from uranium (caused by its radioactivity) by Henri Becquerel in 1896. Although the nature of X-rays and radiation from uranium and the their classification as ionising radiation would not be known for decades, these discoveries were the first two steps into the world of radiation physics [1].

It was very quickly discovered that X-rays could affect the human body. Physicists found that prolonged exposure of skin to X-rays could lead to burns and hair loss. These discoveries along with a few cases that resulted in the death of the X-ray workers involved, had the result of X-rays being treated as potentially dangerous. Similarly, the dangers of radiation from radioactive sources such as Radium were discovered relatively quickly although it took until the end of the 1920s before this was widely known [1].

With the development of particle accelerators and nuclear reactors in the first half of the previous century, it became possible to produce radioactive materials and types of radiation generally not found in nature. This has lead to applications of radiation in industry, medicine and science that could never have been imagined by Röntgen or Becquerel. As the use of radioactive sources in the society increased, accidents involving these sources started to occur and some simply got lost.

An example of the loss of a radioactive source during transport occurred in 1968 when a ^{60}Co source fell from the truck it was being

transported on, between Salt Lake City and Kansas City in the US. As the truck had moved a distance of 1800 km before it was discovered that the radioactive source had been lost, it was decided that the search for the missing source would be conducted using an airplane based system that had been developed for radiological surveys [2, 3]. The system was successfully used to locate a radioactive source which was verified as the missing ^{60}Co source using gamma spectrometry. Although airborne radiation detection instruments had been used for almost two decades [4] to search for naturally occurring sources of ionising radiation, this was one of the first instances where a mobile gamma spectrometric system was used to search for a lost man made radioactive source.

The number of sources considered lost or otherwise unaccounted for have since increased dramatically (e.g. [5] and [6]) and the International Atomic Energy Agency (IAEA) classifies these as "orphaned sources". An accident caused by an orphaned source occurred in Lia, Georgia in 2001 where three people collecting firewood were irradiated by two abandoned radioactive sources that had been used as heating elements in a radioisotope thermoelectric generator [7]. Another event was the result of an improperly disposed of medical radiation therapy source in Mexico in 1984, which was sold as scrap and subsequently melted into rebars [8]. The examples presented here are only a few of many more similar to these [5].

Although most orphaned sources are of a relatively low activity and cases where the ionising radiation from these sources can cause immediate harm are rare, there is an interest in minimising the risk to the public. This means that there exist in a modern society a need for an organisation that can find and safely take care of orphaned sources or sources involved in an accident. However, due to the nature of radioactive sources and ionising radiation, some sources that are potentially dangerous enough to be lethal to a large group of people, can in some cases be impossible to detect only a few centimetres away. Thus there is also a need for ongoing research into developing instruments and methods of locating and identifying radioactive sources more quickly, at larger distances and at a lower cost.

1.2 Aims of this work

The overarching aim of this work has been to improve the probability of detecting radioactive point sources when performing field surveys using mobile gamma spectrometers. This general aim can be divided into

several specific aims applied to one or more of the works presented in this thesis:

- create methods for visualising and processing gamma spectrometric data that has a time and geographic dependence (Paper I and Paper II) which reduces the workload of an operator of the system and thus improves the probability of detection.
- develop methods and detector systems for surveying enclosed areas using mobile measurements (Paper II) and stationary measurements (Paper IV).
- investigate the possibility of using gamma spectrometers as neutron radiation detectors for mobile survey systems (Paper III).
- model and maximimise the probability of detecting radioactive point sources using mobile gamma spectrometry systems (Papers III and V).

Chapter 2

Theory

2.1 Background

2.1.1 Radioactivity and ionising radiation

Almost 120 chemical elements have so far been identified, of which only 94 occur naturally on earth [9]. The chemical element of an atom is decided by the number of protons in the nucleus. For example, an atom with 6 protons in the nucleus is a carbon atom. Most carbon atoms also have 6 neutrons in the nucleus which means that the sum of the protons and the neutrons is 12 and this is called an isotope of carbon, specifically carbon-12 or ^{12}C. An alternative is a carbon atom with 7 neutrons in the nucleus which is the isotope ^{13}C.

The number of neutrons in the nuclei of an isotope can be energetically unfavourable, that is: the nuclei will reach a lower energy state by getting rid of excessive energy. This isotope is thus unstable as it will get rid of the excessive energy by transforming into another chemical element (and isotope), and in the process of doing so, it will emit ionising radiation. A nucleus that transforms from one element to another by reaching a lower energy state undergoes a radioactive decay, and isotopes which can transform in this way are radioactive. For example, ^{14}C is a radioactive isotope that has 8 neutrons and 6 protons. As it is energetically more favourable for a nucleus to have 7 neutrons and 7 protons, ^{14}N decays into ^{14}C, and in the process emits an electron as visualised in Figure 2.1.

Most radioactive isotopes emit two of three common types of radiation when decaying. These types of radiation are alpha (α), beta (β) and gamma (γ). Alpha and beta radiation are particles that are easily

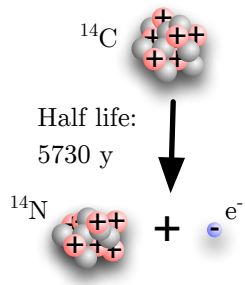

Figure 2.1: The decay of ^{14}C into ^{14}N by the emission of an electron.

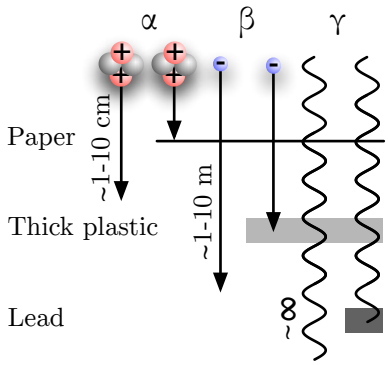

Figure 2.2: The three common types of radiation, alpha, beta and gamma as well as their range in air and what materials are required to stop the radiation. Gamma radiation does have a limited range in air though for many practical purposes, this limitation can be ignored.

stopped by matter and thus have a short range, generally a few centimetres to metres. Gamma radiation is electromagnetic radiation, which is similar to visible light but with much higher energy. The range of gamma radiation in air can usually be approximated as infinite, though in practice the range is limited. The three types of radiation and their range are illustrated in Figure 2.2.

Another type of radiation, which is commonly produced by the splitting of an atom, is neutron radiation. Although the neutron is a particle, it interacts relatively weakly with most matter and is thus hard to detect directly. Neutron radiation does have a tendency to be absorbed by atomic nuclei, for example ^{14}N which is found in air. When this happens, there is a high probability that a high energy gamma ray is emitted, which can be detected by a gamma radiation detector.

The activity of a radioactive source is measured in number of decays per second that is occurring in the source, and the unit is Becquerel (Bq). Thus a source with an activity of 100 Bq undergoes 100 decays per second, while a source with an activity of 10 MBq has 10 million

radioactive decays per second.

2.1.2 Radiation detectors

When searching for radioactive materials, especially over large areas and distances, it is usually preferable to do this using a detector that measures gamma radiation due to the limited range of α and β radiation (see Figure 2.2). The exception being when the radionuclide of interest does not emit any gamma radiation. An important aspect of gamma radiation is that the energy of the radiation is specific to the isotope which is emitting it. For example, the isotope ^{137}Cs emits gamma radiation with the energy 662 keV whereas ^{60}Co emits gamma radiation with two energies, 1173 and 1333 keV. A gamma radiation detector that is able to determine the energy of radiation can thus be used to identify the isotope from which it was emitted.

There are in principle two groups of detectors (able to measure gamma energy) that are in use, scintillation based and semi-conductor based. Scintillation based detectors work on the principle of converting radiation absorbed by the material in the detector into light, the amount of which is proportional to the gamma energy. The light is in turn converted into an electrical pulse, which is amplified in several steps, before it is converted into an energy value which is registered by a computer. These detectors are generally relatively cheap but have a poor energy resolution, i.e., they can not be used to distinguish between two gamma energies close to each other. NaI(Tl) and $LaBr_3$:Ce are two types of scintillation detectors.

Semi-conductor detectors are in principle diodes with a very large volume. When a gamma ray is absorbed by the diode, a small electrical charge is generated across the diode. By back-biasing the diode, the charge can be collected, amplified and converted into an energy value in the detector electronics. Semi-conductor detectors are generally more expensive and smaller than scintillation detectors but have a superior energy resolution and can thus be used to distinguish between gamma energies that have a small energy separation. One of the more common types of semiconductor based detectors in mobile gamma measurements is the high purity Germanium (HPGe) detector.

As these detectors register the energy of the gamma radiation being absorbed in the detector, they are gamma spectrometers. When performing a measurement, the gamma radiation events are divided into energy intervals (bins). By plotting the number of pulses per energy interval as a function of gamma energy, a histogram is created. This

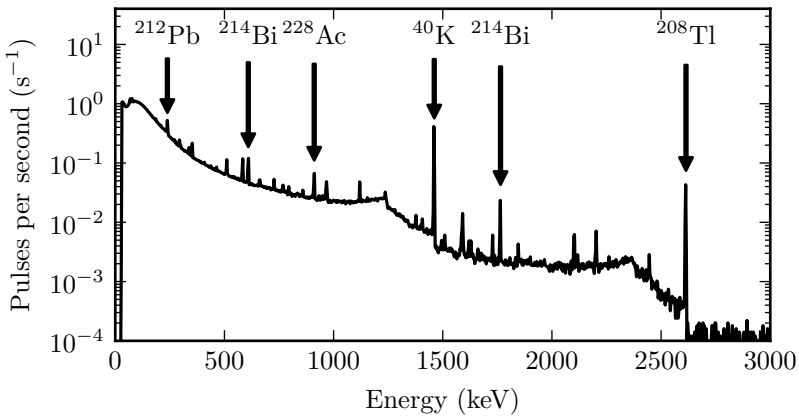

Figure 2.3: A background gamma energy spectrum as measured using a HPGe detector. The peaks represents naturally occurring radioactive materials, some of which are marked.

histogram is a gamma spectrum and an example of this is shown in Figure 2.3, which shows the spectrum of a background radiation measurement (of naturally occurring radioactive materials) using a HPGe detector.

A detector that is turned on and counting pulses in order to create one spectrum does this for a length of time, which is the integration time. For example, a detector can be set to perform two integrations in order to create two spectra with an integration time of 5 s each, and will thus be performing a 10 s long measurement.

The radioactive sources used in the works presented here have a small volume in comparison to that of the detector and can thus be approximated as point sources. This means that the amount of radiation (from the source) registered by the detector can be approximated as decreasing with the inverse square of the distance (ignoring the attenuation of gamma radiation in air), in practice, the area of the sphere with a radius equal to the distance between the two. Thus, in order to maximise the number of pulses registered by the detector, it has to be brought as close to the source as possible.

2.1.3 Statistics

It is impossible to perform a radiation measurement without the detector also registering background radiation. If it is unknown to the operator if a source is present or not, it is thus possible that the background radiation is interpreted as originating from a radioactive source that in practice is not present. Statistics can be used to model radiation measurements and thus calculate the probability of correctly detecting the presence of a point source (true positive) and incorrectly interpreting background radiation as a source (false positive). The problem of determining if a measurement result indicates the presence of a radioactive material or not is what underlies the discussion of statistics in this section.

Consider the following: a radiation detector is set up to measure the radiation from a radioactive source. The detector is turned on for 120 seconds and registers a total of 298 pulses, which gives a pulse rate (or count rate) of ≈ 2.5/s. The integration time however is set to 1 s and the number of pulses registered by the detector during each of the integration periods is shown in the left part of Figure 2.4. The distribution of registered pulses for the 1 s long integration periods is shown in the right part of the figure. The number of random events (pulses) occurring in a (time) interval of fixed length can often be modelled using a theoretical distribution, called the Poisson distribution. The Poisson distribution is thus useful here and it is shown in the figure as well.

As illustrated in Figure 2.5 the Poisson distribution is somewhat skewed and this is especially true for low mean values. The skew is less pronounced for larger mean values which means that in these cases, the normal distribution can be a good approximation of the Poisson distribution as illustrated by the black line in the figure.

Consider a radiation detector that is performing repeated integrations of the naturally occurring background radiation. The number of pulses registered by the detector for each integration follows a Poisson distribution. As there is a possibility that a radioactive source comes near the detector, the operator of the detector wants to set a limit in number of pulses at which the detector is considered to have detected a radioactive source. This value is called the critical limit (C_{L}).

The operator wants the detector to be as sensitive as possible to radioactive sources but setting the limit too low will result in a higher probability of false positives than what the operator find acceptable. For example, a detector system has a background count rate of 5.4 which is thus the mean of the Poisson distribution which describes the number

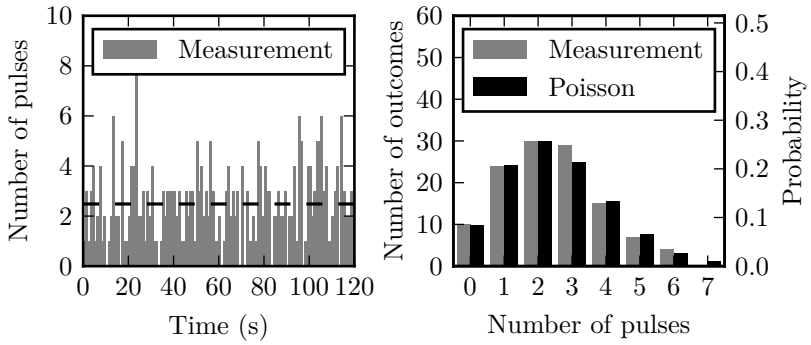

Figure 2.4: The left panel shows the results of performing 120 consecutive one second long integrations with a mean of 2.5 pulses per second as indicated by the black dashed line. The right panel shows the distribution of the results from the measurement in the left panel as well as the theoretical Poisson distribution.

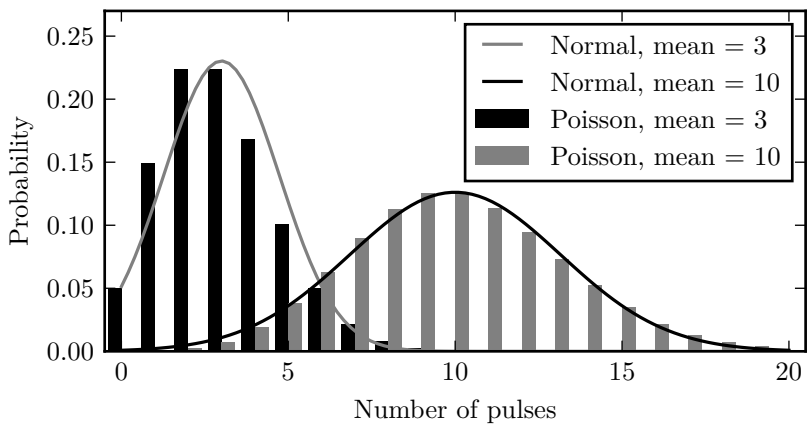

Figure 2.5: The shape of the Poisson distribution compared to the normal distribution for mean values of 3 and 10. In the latter case, the normal distribution is a sometimes reasonable approximation of the Poisson distribution.

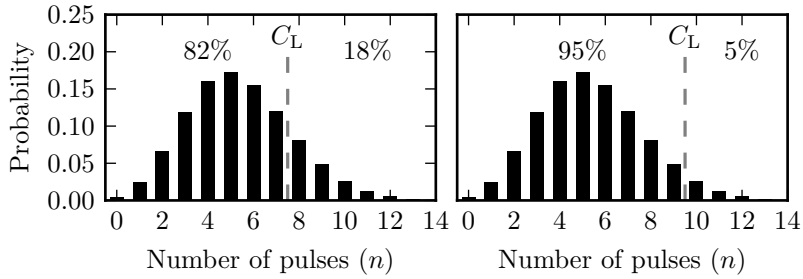

Figure 2.6: The plots illustrate the false positive probability (and true negative probability) when measuring background and using two different critical limits (8 and 10). The plots use a Poisson distribution with a mean value of 5.4.

of counts registered by the detector for every 1 s long integration. The operator sets a critical limit of 8, which results in the system indicating a source in 18% of the integrations when only measuring background radiation. This is illustrated in Figure 2.6.

The operator determines instead that an acceptable false positive probability (when measuring background) is at most 5%. Thus he has to find an outcome (in Figure 2.6) at which the probability of getting that value or a greater one is less than 0.05. The resulting critical limit is in this case found to be 10 as, illustrated in the right panel of Figure 2.6.

A radioactive source with an activity of 500 Bq (decays per second) is placed near the detector mentioned in the previous paragraph and the mean value of the number of pulses registered by the detector changes to 7.9, which means that the source provides on average an extra 2.5 pulses per integration in the detector as shown in the top panel of Figure 2.7.

The figure illustrates that when measuring a 500 Bq source, the probability of detecting it is 27%. However, the operator wants to find a pulse rate (and source activity) where the (true positive) probability of detecting the source is 95%. The source activity where this is true is called the detection limit or minimum detectable activity.

Thus a mean value of the Poisson distribution (representing a specific source activity) has to be found where 95% of the area of the distribution is above the critical limit (C_L). This value is found to be 15.7 (as illustrated in the lower panel Figure 2.7) which represent a source activity of 2060 Bq and this is thus the detection limit.

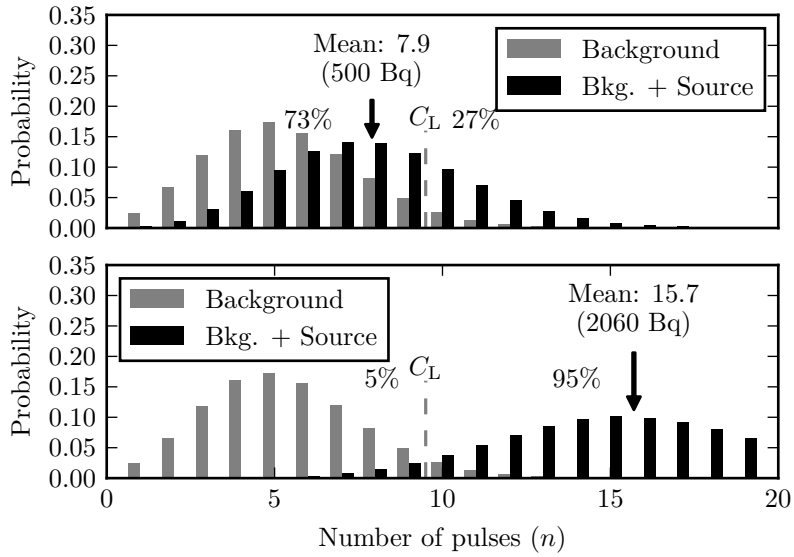

Figure 2.7: The plots illustrates the probability of detecting a radioactive source for a given critical limit and source activity. The background distribution is shown as a comparison to the source measurement distribution but the percentage values are the probabilities of an outcome below or above the critical limit when measuring a source. The bottom panel illustrates the detection limit of the system (2060 Bq), if the true positive probability is set to 95% (as mentioned in the text).

2.2 Mobile measurements

Consider an area that is believed to contain a radioactive source that needs to be found and taken care of. If unlimited time and resources are available to search this area, any gamma spectrometer can be used in the search as the detector can be moved in infinitely small steps. This ensures that in at least one of the measurement points, the detector is close enough to the source that it will be detected.

In practice, resources are limited and only one or a few detector systems can be used for a limited time to search a given area. Thus the detector systems that are used have to be moving at a speed and along routes dictated by the resources available.

Given that the source is well below the limits of detection in most

of the area being surveyed, if the detector uses an integration time as long as the total measurement time, the pulses counted by the detector will be almost only background pulses. This will in most cases make it impossible to determine if a radioactive source is present and even if the activity of the source is high enough to yield a peak in the spectrum, it will be impossible to determine the approximate location of the source. Thus, in order to improve the sensitivity and to provide some spatial information in the measurement, it must be split into several integration periods.

Although every integration period will yield a spectrum, if the source is at the limits of detection, it will not be possible to discern a peak in the spectrum as caused by a radioactive source (compare to Figure 2.3). Instead the number of counts in an energy region can be counted and compared to the number of pulses that are expected if the detector is measuring only the background (see section 2.1.3). For example, when using a NaI(Tl) detector to search for a ^{137}Cs source, the number of counts registered by the detector in the region (ROI) between 630 and 690 keV can be extracted.

Which integration time to use in mobile gamma spectrometry measurements is decided based on desired spatial resolution, background count rate, desired sensitivity, speed of the detector system and assumed minimum distance between the detector and the source. If spatial resolution in the measurements is ignored and maximum sensitivity is set as a goal, a relation between integration time, speed and source to detector distance can be created.

If the detector is moving slowly or the detector has a relatively long minimum distance to the source, the time that the detector spends in its "vicinity" will be longer and longer integration time yields a higher sensitivity. If the detector is instead moving quickly or the minimum distance between the detector and source is short, a shorter integration time will result in a higher sensitivity as less of the background will be counted. Similarly, if the background count rate is higher, the detector system will have a higher sensitivity when using a shorter integration time whereas a lower background count rate favours a longer integration time. This is summarised in Table 2.1.

An integration time that is often used is $\sim$ 1 s (e.g. [10–14]) with the motivation that as mobile measurements are paired with GPS coordinates, shorter integration time allows for a higher spatial resolution in the data with which to pinpoint the location of a potential radioactive source. However, several authors do suggest integration periods of 5–10 s or more [15–17], with the argument that this improves sensitivity.

	Bkg. high	Bkg. low
Speed fast Dist. long	Short	Long
Speed fast Dist. short	Very short	Short
Speed slow Dist. long	Long	Very long
Speed slow Dist. short	Short	Long

Table 2.1: The relation between optimal integration time, background count rate, detector movement speed and minimum source to detector distance. Integration times are marked as "short" or "long", with the possibility of being prefixed with "very".

One potential solution to improving the sensitivity of a mobile gamma spectrometry system is to simply use detectors with a large volume. A large volume results in a higher probability of a gamma ray from a radioactive source interacting with it. However, a detector with a large volume will also have a high weight which can be a limiting factor in some measurement set-ups. A backpack based survey system, for example, commonly uses ⌀7.6 by 7.6 cm^3 detectors [17–20] as any larger and heavier detectors can be cumbersome to carry for long periods, as discussed in Paper II. Furthermore, although the probability that a gamma photon will be registered is increased as the volume of the detector is increased, the probability that the detector will register background gamma radiation also increases. Thus at some detector size, the background count rate will increase faster than the count rate from a radioactive source and thus the sensitivity will decrease [21]. This means that car borne and airborne survey systems are generally not limited in size because of weight. Instead, detector volumes are picked in order to maximise sensitivity and thus common detector volumes used in vehicles are 4, 8 and 16 l [22–24].

Background radiation levels are not constant, which is an important factor in mobile gamma spectrometry measurements. As the background radiation is primarily caused by naturally occurring radioactive elements (potassium, uranium and thorium), the radiation levels from these sources can in some cases change by an order of magnitude over a distance as short as a tens of metres [25, 26]. This change in background count rate can be caused by, for example, localised concentrations of naturally occurring radioactive materials in rocks or by shielding of these materials when passing over water.

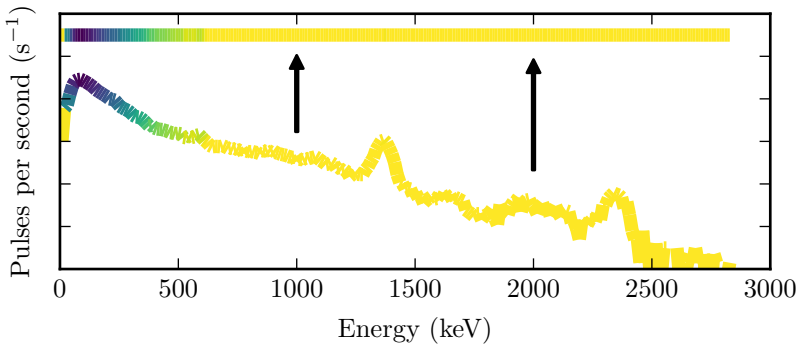

Figure 2.8: Illustration of colour coding of a spectrum from a NaI(Tl) detector.

One method for taking a changing background into account is to assume that the background radiation levels are changing slowly and assume that the background in the current integration period is approximately the same as the mean background count rate the past minutes (Paper I). Another method is to use knowledge of the location of peaks in the gamma spectrum to strip away the background (e.g. [12, 23, 27, 28]). Cresswell and Sanderson suggests a method of filtering the data [29] and Kock et al. uses previous surveys of the area to compensate for background radiation levels [25].

2.2.1 The deviation display

Though it is certainly possible for the operator to look at each individual spectrum registered by the detector system, this is time consuming. Showing several spectra at the same time can also be problematic and lead to clutter due to the two dimensional nature of a spectrum. However, instead of showing a spectrum as a two dimensional plot, it can be colour coded and thus be reduced to one spatial (and one colour) dimension, as illustrated in Figure 2.8.

The colour coded lines can then be stacked in a colour coded image, showing time and gamma energy on the x and y axis as well as the amplitude on the colour scale, as illustrated in Figure 2.9. Visualising three dimensional data as a colour or intensity coded image, commonly called rainbow plot or waterfall plot in mobile gamma spectrometry, has a long history [30]. The simple version of this type of plot, as described above, was investigated as a tool for mobile gamma spectrometry by Aage et

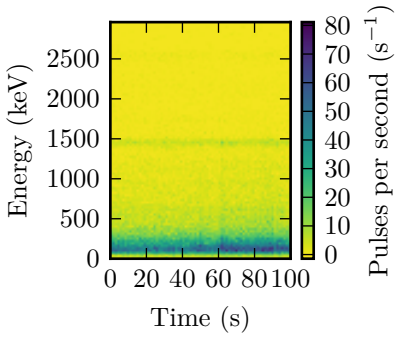

Figure 2.9: A simple rainbow plot of several consecutive spectra with an integration time of 1 s using a NaI(Tl) detector.

al.[12]. Alternatives based on more complex methods of analysing spectrometric data has also been used by Cresswell and Sanderson [29].

If the number of pulses in a an energy range (region of interest, ROI) from several spectra is observed, it is expected that it has a Poisson or normal distribution around a mean value as explained in Section 2.1.3. Having determined the mean value as well as the distribution from several spectra, a critical limit can be set. This can be done for small ROI:s (only a few keV wide) and repeated for the whole spectrum. Figure 2.10 illustrates how a mean spectrum as well as the corresponding critical limit can be determined. In the example illustrated in the figure, this is done for 100 consecutive spectra with an integration time of 1 s using a mobile NaI(Tl) based survey system.

As values below the critical limit are considered background, only values above are of interest. Specifically, the amount that a value exceeds the critical limit is of interest as it relays the probability that a source has been found. Thus, by comparing a spectrum to a critical limit, the amount that the spectrum exceeds the critical limit can be plotted as illustrated in Figure 2.11. By colour coding these results (similar to Figure 2.8) and placing many such consecutive results side by side, the deviation display is created.

When performing the calculations required to create the deviation display, using Poisson distributions to model the distribution of pulses around the mean value can be problematic due to the required computational power. For this reason, normal distributions can be used as an approximation. A thorough explanation of the mathematics behind the use of normal distributions to solve the problem can be found in Paper I. Paper II also discusses the problem and presents an alternative that uses a method for suppressing noise in the parts of the spectrum where the

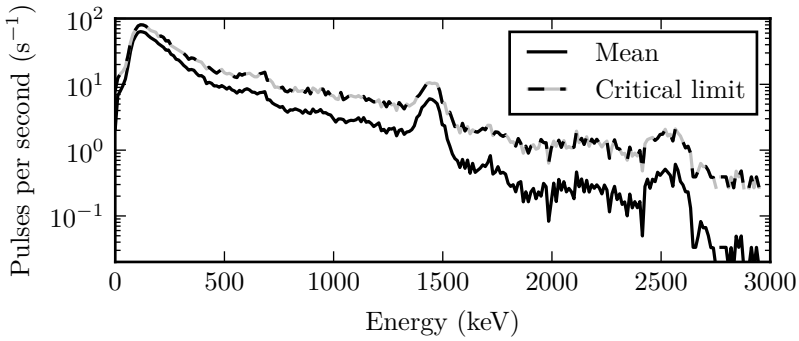

Figure 2.10: The mean spectrum from 60 consecutive 1 s integration periods measured using a mobile NaI(Tl) based survey system and the critical limit extracted from the same data set, using a false positive probability of 2%.

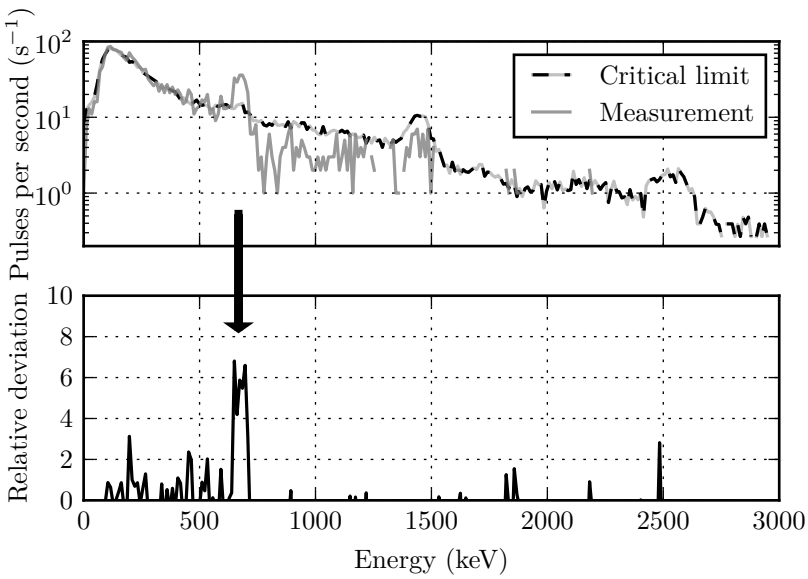

Figure 2.11: The top panel shows a comparison between a critical limit and a spectrum produced when the detector system measured a ^{137}Cs source. The bottom panel shows the relative positive difference between those two.

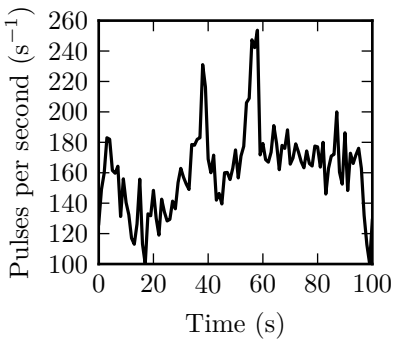

Figure 2.12: The number of pulses in the ^{40}K ROI (approximately 1370–1550 keV) of a NaI(Tl) detector system as it passes several concrete buildings.

pulse rate (and mean) is low and thus the normal distribution is a poor approximation of the Poisson distribution.

2.2.2 Map visualisation

As gamma spectrometers have a limited energy resolution (mentioned in Section 2.1.2) and because the integration times in mobile gamma spectrometry are short, it is useful to sum the number of pulses over a relatively wide region of interest (ROI) and perform calculations on this value. Several methods for processing ROI data exist, for example stripping (e.g. [12, 23, 27, 28]), and high energy to low energy comparison [15]. Visualising the unprocessed or calculated values can be done by simply creating a plot showing the data as a function of time. This is illustrated in Figure 2.12, which shows the number of pulses per second in a ^{40}K ROI (approximately 1370–1550 keV) as a NaI(Tl) detector system passes several buildings.

It is usually appropriate to a mobile gamma spectrometry operator to visualise ROI data by colour coding it and plotting it on a map. However, doing this can lead to a problem where a few markers in the map representing a data point with a large value are covered by many markers representing a smaller value. The solution to this problem is to sort the rendering order of the dots on a map by the value they represent. Thus markers representing high intensity values are rendered last and will thereby be easier to find. Both the problem and the solution are discussed in Paper II.

2.2.3 Optimisation of region of interest

As described in Section 2.1.3 and illustrated in Figure 2.6, the background radiation has to be taken into account when deciding on a critical limit. The number of background pulses registered is partially a factor of the width (energy range) of the ROI that is used. Using a ROI that has a wide energy range in comparison to the width of a peak in a spectrum (Figure 2.3) will result in a worse signal to background (noise) ratio. However, using a narrow energy range might result in too few pulses being registered to reach or exceed the critical limit set for that energy range. Thus there should be an optimal energy range for a ROI, that maximises the probability of detecting a source.

The optimal energy range can be determined by starting with a small energy range and calculate the probability of detecting a radioactive source using that ROI. If the ROI is then expanded step by step until the probability of detecting the source decreases, the optimal energy range has been fund. A more thorough explanation of the algorithm, and its application to optimise a NaI(Tl) detector for locating neutron sources, is discussed in Paper III.

2.2.4 Modelling moving sources

Assume that a detector, performing a mobile gamma spectrometry survey, is moving along a perfectly straight and flat road. The position of the detector on the road is a function of time (t). Some distance from the road, a radioactive source is located and the detector passes the source (it is at its closest to the source) at time τ. It is possible to create a mathematical expression ($\lambda(t)$) that yields the instantaneous count rate of the detector as it passes the source and that in effect provides the probability that a gamma photon emitted by the source is detected by the survey system. An example of the shape of the curve showing the instantaneous count rate for a detector moving at 1 m/s past a source 1 m away from the path the detector is moving along is shown in Figure 2.13.

As mentioned previously, a mobile gamma spectrometry system performs repeated integrations (of length δ, usually $\sim$1 s) when surveying for radioactive sources. This means that Figure 2.13 is chopped up into parts where the area under the curve of each part represents the number of pulses expected to be registered in that integration period. The alignment of the integration periods in relation to the location of the source can usually not be controlled. Thus the actual area under the curve can not be known beforehand either. There are however two extreme

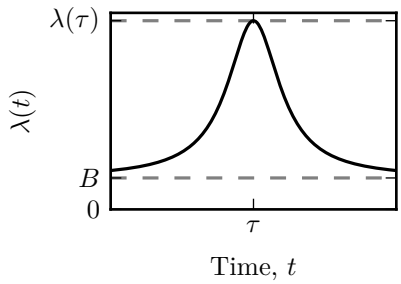

Figure 2.13: The general shape of the curve describing the instantaneous count rate in a detector passing a radioactive source. Adaptation of a figure shown in Paper V.

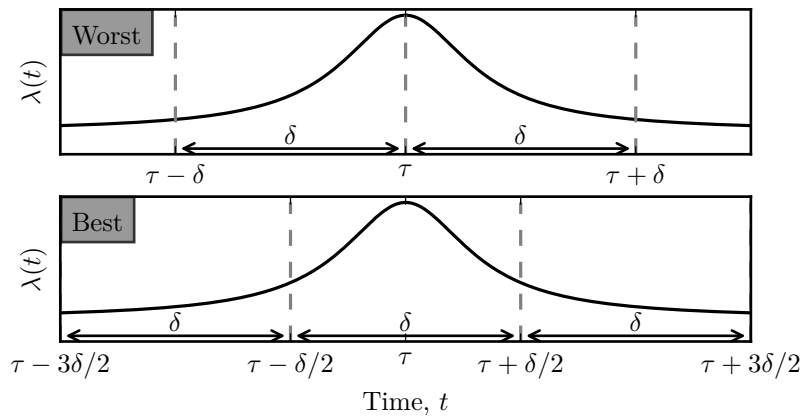

Figure 2.14: The general shape of the distribution describing the count rate in a detector passing a radioactive source as well as markings indicating the best and worst case scenarios of alignment of integration periods. Adaptation of a figure shown in Paper V.

values that represent the greatest area and the smallest area under the curve. These extremes also represent the highest and lowest probability (best and worst case) of finding the source. The best and worst case is illustrated in Figure 2.14.

Similar to how there is an optimal ROI energy range, as mentioned in the previous section, there is also an optimal integration time where the probability of detecting a radioactive source is the highest. Similar the the method for determining the optimal ROI, the optimal integration time is found by first calculating the probability of finding a radioactive source when the integration time is short. The calculation is then repeated for a slightly longer integration time. By calculating the prob-

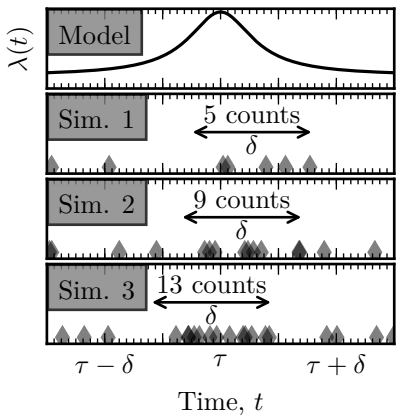

Figure 2.15: The top panel represent the distribution that describes the probability of a moving detector detecting radiation from a stationary source (see Figure 2.13). The next three panels illustrates simulated measurements and the maximum number of counts achieved using an integration time of 1 s. Adaptation of a figure shown in Paper V.

ability of detecting a source for an increasing length of the integration time until the probability starts to decrease, the optimal integration time is found. Using this method, it is also possible to determine the minimum detectable activity for a given false positive probability (critical limit) and false negative probability (not detecting the source when it is present).

One complicating factor when performing these calculations is that although the probability of finding the source is the highest for the integration period that has the largest area (see Figure 2.14), the probability of finding the source in adjacent periods is not zero. Thus when calculating the probability of detecting the source, the probability of finding the source in any of the integration periods near the peak of the curve (Figure 2.14) have to be included.

An alternative to mobile gamma spectrometry systems that perform repeated short integrations is one that logs every individual pulse registered by the detector as a gamma energy with a timestamp of the pulse [11, 31]. A detector operating in this way is performing "list mode" measurements. Using list mode measurements, it is possible to recreate every possible alignment of the integration periods.

Due to the nature of pulse statistics, it is unlikely that the largest number of pulses registered by the detector will fall within the best case integration period. Thus when using list mode measurements, the maximum number of counts for a given integration time is found, as illustrated in Figure 2.15.

By testing a range of integration times for the three measurement scenarios mentioned above, in order to determine the optimal integra-

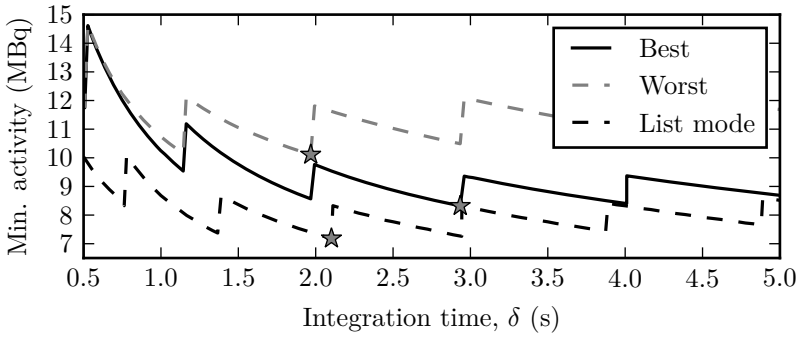

Figure 2.16: An example of a plot showing the minimum detectable activity for a specific radionuclide given a specific set of measurement parameters when performing a mobile survey. The stars indicate the lowest valley for each curve and thus the optimal integration time and minimum detectable activity. Adaptation of a figure shown in Paper V.

tion time and thus the highest possible sensitivity, a figure similar to Figure 2.16 will be the result. As the integration time increases, in order to keep the false positive probability relatively constant, the critical limit (C_{L}) will also have to be increased. Because the detector can only register discrete events the critical limit is an integer value. This causes a sawtooth pattern as exemplified in the figure.

When performing a mobile survey, it is more useful to set the critical limit based on the number of acceptable false positives per hour instead of the probability of a false positive for a single integration period. This means that as the integration time increases, the false positive positive probability also increases in order to keep the rate of false positives per hour constant.

Though the mathematics behind the models described here were touched upon by Long and Martin [32], they were first put to use in calculating sensitivity values for mobile gamma spectrometry systems in Paper III. The mathematics was then extended and generalised to make it into a set of useful models and algorithms in Paper V.

2.3 Measuring neutrons with gamma detectors

Neutron radiation can be hard to detect directly as neutrons do not have an electric charge. Thus neutron detectors have generally been based on

the conversion of neutron radiation to other types of radiation which are easier to detect [33, 34]. For example, when a neutron is absorbed by a ^{3}He nucleus, it will decay into a ^{3}H nucleus by the release of hydrogen nucleus and 0.764 MeV of energy. This reaction can be readily detected if enclosed in a radiation detector. Due to the high probability (cross section) of ^{3}He absorbing neutrons, detectors based on this principle are one of the more common for detecting neutrons [35].

^{3}He gas is a byproduct of the production of nuclear weapons [36] and thus the price has increased dramatically the past decades which is why alternatives to the nuclear process described above have been investigated. One such alternative is the use of polyvinyl chloride (PVC)[37–40]. Chlorine has a relatively high, though still much lower than ^{3}He, cross section for absorbing neutrons that results in the emission of high-energy gamma rays which can be detected by a regular gamma spectrometer. Also present in the PVC is hydrogen and although the cross section for neutron absorption in hydrogen is relatively small, the cross section for neutron scattering against the hydrogen nucleus is high and this reduce the energy of the neutron which further increases the cross section of chlorine.

Another important factor to take into consideration is that most types of neutron sources (e.g. ^{241}AmBe, ^{252}Cf/^{250}Cf, ^{238}Pu$-^{13}$C) also emit high energy gamma radiation which is easy to distinguish from natural background radiation and thus making it possible to detect such sources by this radiation.

Paper III discuses the use of PVC covered NaI(Tl) detectors as neutron radiation detectors in mobile measurements. This type of neutron detector is also compared with a standard ^{3}He based neutron detector intended for car-borne use.

2.4 Iterative image reconstruction

Bringing the detector as close as possible to the radioactive source will generally improve the probability of detecting it, as mentioned in Section 2.1.2. In some cases however, this is not desirable or possible. If for example the activity is high enough that the presence of a source can be detected from a large distance (e.g. 100 m) then regular mobile survey systems can not be used to pinpoint the location of the source as the detector will be overwhelmed by the high count rate when moved too close. Furthermore, debris, other obstacles or threats to the operator might prevent a close approach to a radioactive source in order to

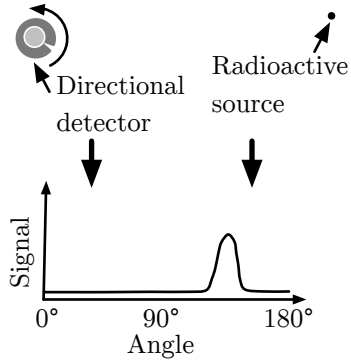

Figure 2.17: Illustration of the use of a directional gamma radiation detector to scan over a radioactive source.

pinpoint it.

One solution to this problem is to use a directional detector, i.e. a detector that is more sensitive to radiation in one direction than another. By slowly rotating the detector and recording the count rate registered by the detector, the direction to a radioactive source can be determined as illustrated in Figure 2.17. In order to determine the location of the radioactive source, this procedure has to be repeated in at least one more location.

If more than one radioactive source is present in the area that is being surveyed, more than two locations might be required to determine the locations of the sources. It also becomes harder for the operator to determine the angle at which the directional detector points towards the radioactive source if the angular resolution of the detector is limited. These problems can be solved by using an image reconstruction algorithm, similar to the algorithms used in diagnostic medicine [41], that produces a map of the distribution of the sources in an area based on data from angular measurements. The algorithm is iterative as it can be repeated as necessary and should, in principle, improve the result for every additional iteration that it is run. The algorithm works roughly as follows:

1. Assume a uniform distribution of the radioactivity in the area of interest.

2. Simulate the measurements of the assumed radioactivity distribution at locations and angles corresponding to those of the real measurements.

3. Compare the simulated measurements with the actual measurements by dividing the curve of the actual measurement with the curve from the simulated measurements.

4. Modify the assumption based on the comparison.

5. Go to step 2.

A system as described here, will be a compromise between angular resolution and counting efficiency. However, if the angular resolution of such a detector system is well characterised, it is in theory possible to extract a higher angular resolution from low resolution data using deconvolution [42, 43]. In order to do this, the response of the system when measuring a point (source) has to be determined and this response is called a point spread function (PSF). The method for extracting higher resolution data from lower resolution data using a PSF is discussed in Paper IV.

The resolution of a system is commonly defined as the full width at half maximum (FWHM) of a peak in the data from measuring a point (-source). This definition can be used to determine if two peaks can be distinguished from each other. However, this definition is usually only useful if the peaks have a well defined maxima as is the case where the peaks have a normal distribution. If this is not the true, an alternative exist that is based on finding the separation between two peaks at which the valley is at 10% of the maximum [44, p. p88]. The two methods of determining resolution are illustrated in Figure 2.18 and both definitions as well as their use are discussed in Paper IV.

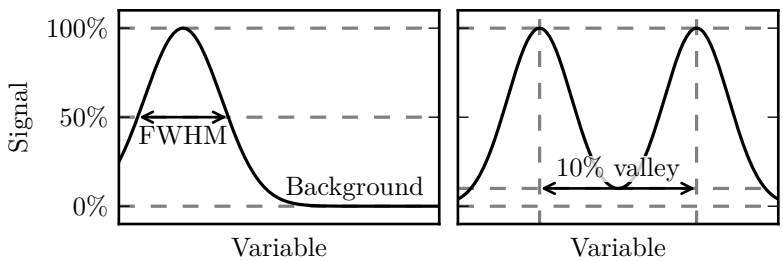

Figure 2.18: Two methods for determining the resolution of a (gamma spectrometric) system. The full width at half maximum (FWHM) method is shown in the left panel and the 10% valley method shown in the right panel is the peak separation at which the valley is at 10% of the maximum value above the background.

Chapter 3

Materials and methods

3.1 Detectors

All in all, 5 different detector systems were used in the research presented here. Four of the detector systems are gamma spectrometry systems (see Table 3.1) and one is a neutron detector system. Though some of the properties of the individual detector systems are discussed in Paper I to V, this section gives an overview of all of the detectors. A short description of each of the detectors, follows.

Table 3.1: List of gamma spectrometric systems used in this thesis and their technical information. Due to the shape of the 4 l NaI(Tl) system, its efficiency is not listed.

	Detector system			
	1	2	3	4
Type	HPGe	NaI(Tl)	NaI(Tl)	$LaBr_3$:Ce
Volume (l)	0.48	0.35	4	0.35
Efficiency [45] (%)	123	100	n/a	135
Resolution[a] (%)	0.15	7.5	7.5	3.0
Electronics	DigiDART	DigiBASE	DigiBASE	DigiBASE
Used in paper	I, II, IV	I, II, V	III	II

[a]FWHM of the 662 keV ^{137}Cs peak.

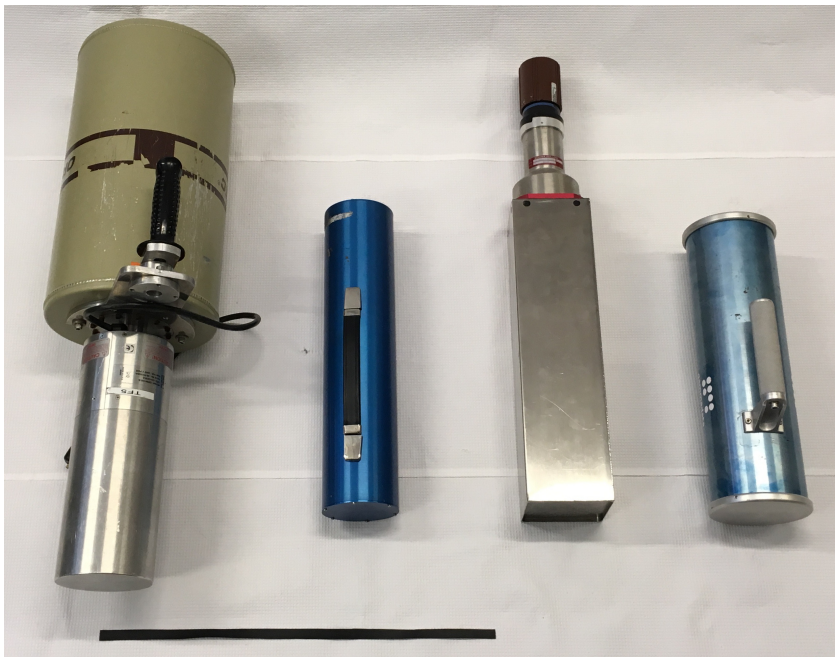

Figure 3.1: The four gamma spectrometry systems used in the research presented here. From left to right: 1. HPGe, 2. ∅7.6 by 7.6cm^3 NaI(Tl), 3. 4 l NaI(Tl) 4. $LaBr_3$:Ce. Note that the 4 l NaI(Tl) detector has been removed from its outer container. The black ruler in the foreground has a length of 50 cm.

3.1.1 Detector system 1, HPGe

High purity germanium (HPGe) detectors are currently the type of gamma spectrometer that offers the highest energy resolution (peaks with the smallest width), and thus has the best ability to distinguish between radioactive isotopes. The HPGe detector used in this research has a relatively large volume in comparison to other HPGe systems and has an efficiency of 123% relative to that of a ∅7.6 by 7.6 cm^3 NaI(Tl) detector when counting the 1333 keV gamma ray emitted by ^{60}Co [45]. The detector has to be cooled using liquid nitrogen which requires the use of a dewar and thus the system has a large volume and is quite heavy with a weight of approximately 20 kg when newly refilled with liquid nitrogen. Figure 3.1 shows the size of the HPGe detector in comparison to

the other detectors. The HPGe detector was used in Paper I, II and IV.

3.1.2 Detector system 2, ∅7.6 by 7.6 cm^3 NaI(Tl)

Thallium doped sodium iodine (NaI(Tl)) is a scintillation material discovered in the 1940s [46, 47] and is still one of the best scintillation materials for use in mobile gamma spectrometry due to its combination of high efficiency and energy resolution in comparison to many other scintillation materials [48]. This particular NaI(Tl) detector has a cylindrical shape with a diameter of 7.6 cm and length of of 7.6 cm, which is a de facto standard size for scintillation detectors. The detector system, encased in an aluminium tube containing the scintillator as well as the electronics, is shown in Figure 3.1. This NaI(Tl) detector was used in Papers I, II and V.

3.1.3 Detector system 3, 4 l NaI(Tl)

A positive aspect of NaI(Tl) is that it is possible to produce a large sized detector from this material, something which is not possible with HPGe. This detector, with a volume of approximately 4 l (10 by 10 by 40 cm^3), is useful when a very high efficiency is required. However, the high weight of the system (approximately 30 kg) does limit its use to stationary or vehicle borne applications. This particular detector was used in Paper III and the detector without its outer cover can be seen in Figure 3.1.

3.1.4 Detector system 4, ∅7.6 by 7.6 cm^3 $LaBr_3$:Ce

Cerium doped lanthanum bromide ($LaBr_3$:Ce) is a recently discovered scintillation material [49], that offers a higher energy resolution and higher relative efficiency than a NaI(Tl) detector of the same size. However, the detector also contains small amounts of radioactivity [50, 51] which gives it worse sensitivity than a similar sized NaI(Tl) detector in many natural background radiation environments [52]. This particular detector is also cylindrical with dimensions ∅7.6 by 7.6 cm^3. The detector in its aluminium tube can be seen in Figure 3.1. It was used in Paper II.

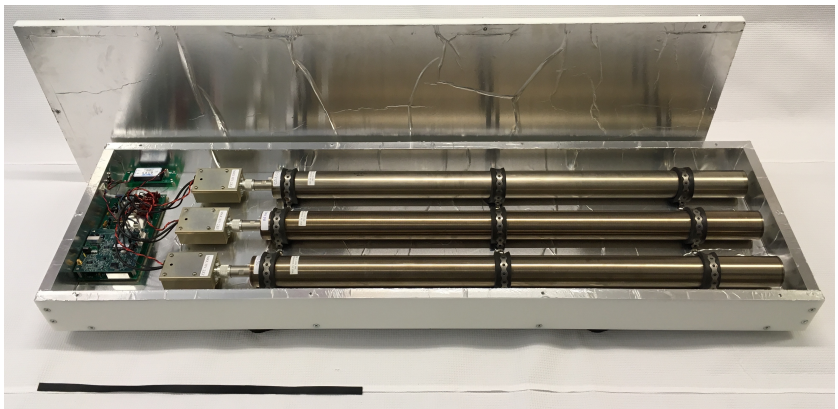

Figure 3.2: The neutron detector used in Paper 3 with the cover removed and showing the 3 ^{3}He tubes. The black ruler in the foreground has a length of 50 cm.

3.1.5 Detector system 5, ^{3}He neutron detector

The 4 l NaI(Tl) detector (detector system 3) used as a neutron detector in Paper III was compared to a dedicated ^{3}He based neutron detector intended for mobile surveys. This type of detector operates under the principle described in Section 2.3. The detector itself consist of 3 ^{3}He tubes, with a total volume of 4.7 l, mounted in a plastic case as seen in Figure 3.2. The plastic case contains a relatively large fraction of hydrogen which slows down the neutrons passing through it and thus increases the probability that the neutrons will interact with the ^{3}He.

3.2 Radioactive sources

When testing the models and equipment presented in this thesis, the use of radioactive sources with properties appropriate for controlled experiments are required. For gamma spectrometry measurements, one of the common radionuclides in use is ^{137}Cs. Its relatively long half-life of 30 years means that a radioactive source of this isotope does not require frequent replacement and as it only emits a single gamma energy of 662 keV it is easy to distinguish from natural background radiation or other radioactive sources. Figure 3.3 shows the spectra from HPGe, NaI(Tl) and $LaBr_3$:Ce detectors measuring a ^{137}Cs source.

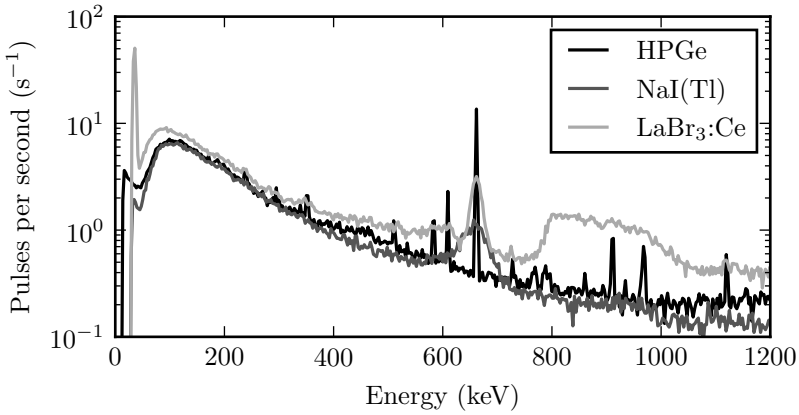

Figure 3.3: The result of using a HPGe, NaI(Tl) and $LaBr_3$:Ce detector to measure a ^{137}Cs source. Note the peak at 662 keV.

For energy calibration, man made radioactive sources such as ^{137}Cs and ^{60}Co can be used. However, as most gamma spectrometers used in mobile gamma spectrometry are relatively large in order to detect radioactive sources that are far away, the background count rate from naturally occurring radioactive materials is generally enough to perform an energy calibration. These materials include ^{40}K which emits gamma radiation with an energy of 1461 keV and ^{208}Tl which emits gamma radiation with an energy of 2614 keV. Figure 3.4 shows backgrounds measurement done using the three detector types. Note that the internal radioactivity is clearly visible in the spectrum from the $LaBr_3$:Ce detector.

For Paper III, the use of sources of neutron radiation was required and three different types were available. The first was of type ^{252}Cf/^{250}Cf, which emits neutrons as it spontaneously undergoes nuclear fission. A ^{241}AmBe neutron source was also used, which emits neutrons when alpha radiation from ^{241}Am hits a ^{9}Be nucleus:

$$^{9}\mathrm{Be} + \alpha \rightarrow {}^{12}\mathrm{C}^{*} + \mathrm{n} + 5.7\ \mathrm{MeV}$$

The excited carbon nucleus also emits a gamma photon with an energy of 4.44 MeV. Similarly to the ^{241}AmBe source, the ^{238}Pu$-^{13}$C source emits a neutron through a nuclear reaction caused by the absorption of a alpha particle in a lighter element (^{13}C):

$$^{13}\mathrm{C} + \alpha \rightarrow {}^{17}\mathrm{O} \rightarrow {}^{16}\mathrm{O} + \mathrm{n} + 2.2\ \mathrm{MeV}$$

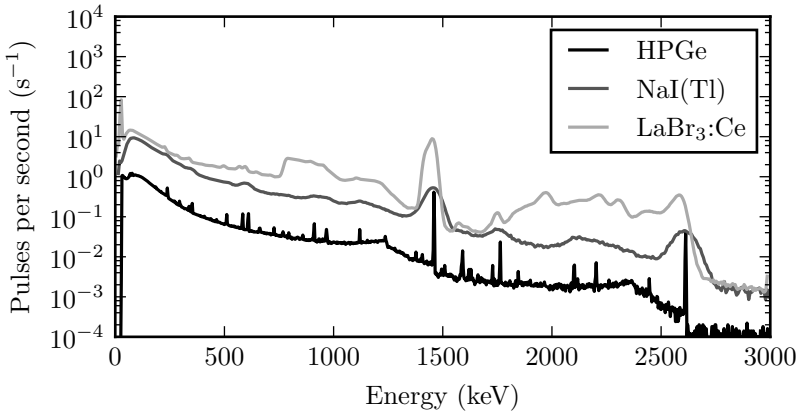

Figure 3.4: A background measurement using the HPGe, NaI(Tl) and $LaBr_3$:Ce detector. The 1461 keV peak from ^{40}K and 2614 keV peak from ^{208}Tl are easy to discern in the HPGe and NaI(Tl) measurement but are hidden in $LaBr_3$:Ce measurement due to its internal radioactivity which produces peaks at those energies [50].

Table 3.2: Neutron sources used, their activity, neutron emission rate and mean neutron energy.

Source	Activity	n emission rate (10^6s$^-$1)	Mean n energy (MeV)
^{241}AmBe	18.5 GBq	1.1±10%	4.4 [53]
^{252}Cf/^{250}Cf	7 + 200 MBq	1.2±30%	2.1 [54]
^{238}Pu−^{13}C	$\sim$ 20 GBq	0.12±30%	$\sim 3-4$ [55, 56]

Common for all these sources is that they also emit high energy gamma radiation as mentioned in Section 2.3, a fact which was used in Paper III. Figure 3.5 shows gamma spectrometry measurements of the neutron sources. Table 3.2 display activity, neutron emission rate and mean neutron energy.

3.3 Deviation display tests

Testing of the deviation display was done using detector system 1 and 2 (Papers I and II) as well as detector system 4 (Paper II). The systems

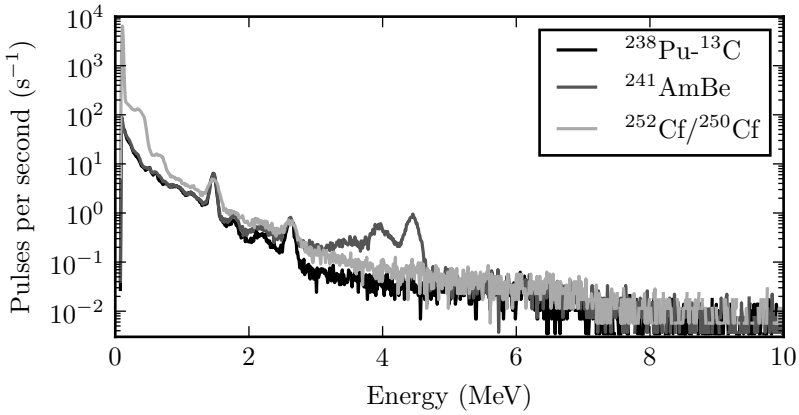

Figure 3.5: Measurements of ^{252}Cf/^{250}Cf, ^{241}AmBe and ^{238}Pu$-^{13}$C sources using detector system 3 (4 l NaI(Tl)). Note that much of the gamma radiation caused by neutron sources is above 3 MeV.

were set to perform repeated 1 second long integrations. As the method requires some knowledge of the background, the detectors performed background measurements for 1 min or longer before the actual tests were started. The detector was then moved past a 60 MBq ^{137}Cs source at a speed of 30 km/h and minimum source to detector distance of $\approx$ 30 m.

From the collected data, both regular waterfall plots and deviation displays were created and compared. As a modification of the deviation display was created for Paper II, the new version was also compared with the old version.

3.4 Backpack measurements

When surveying limited areas for radioactive sources, using a backpack system can be a good option. For this reason detector systems 1, 2 and 4 were tested in a backpack configuration. The system used a GPS for collecting positional information as well as a computer that was used to store the collected data from the detector and GPS. The detector systems were set to perform 1 s integrations in order to achieve a good spatial resolution. Experiments were first done in a controlled environment in an area of 20 by 20 m^2 that was surveyed by walking lines with a 1 m separation. The first survey was a background measurement which

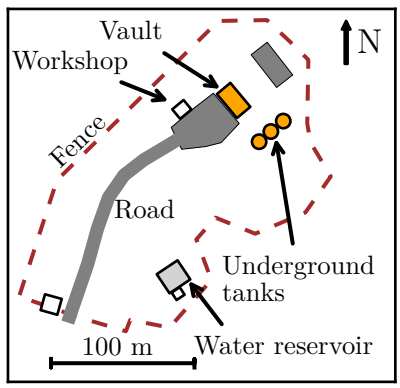

Figure 3.6: A map of the site in Georgia, containing a radioactive waste repository, which was used for the field tests of detector system 1 and 4. Adaptation of a map shown in Paper II.

was then followed by a survey of 3 ^{137}Cs sources placed on the ground in a triangular pattern in the area. Three sources were used in order to test the detector systems in a realistic measurement scenario.

Based on the results of these experiments, detector system 1 and 4 were tested in the field. This was done at a site of a radioactive waste repository in Georgia (in the Caucasus region of Eurasia). The size of the area was on the order of $\sim 10^4$ m^2 and because of the size as well as the terrain, the distance between walking lines was ~ 5 m. A map of the area used to conduct the field tests is shown in Figure 3.6.

Analysis of the laboratory measurements were done by extracting the ^{137}Cs signal from the data and interpolating these results (using the GPS data) over the surveyed area. The area in which the sources could be considered to be detected were compared between the detector. This was done by testing at which detection limits the sources could be considered to be detected.

Due to the size of the area surveyed in Georgia and the distance between walking lines, the analysed data was plotted as individual measurement points on a map of the area. Region of interest count rates plotted included (but were not limited to) ^{137}Cs, ^{60}Co and naturally occurring radioactive isotopes. Paper II holds more information on the controlled experiments and field tests mentioned here.

3.5 Moving detectors

The mathematical models and algorithms used to calculate the sensitivity of mobile gamma spectrometry systems (as described in Section 2.2.4)

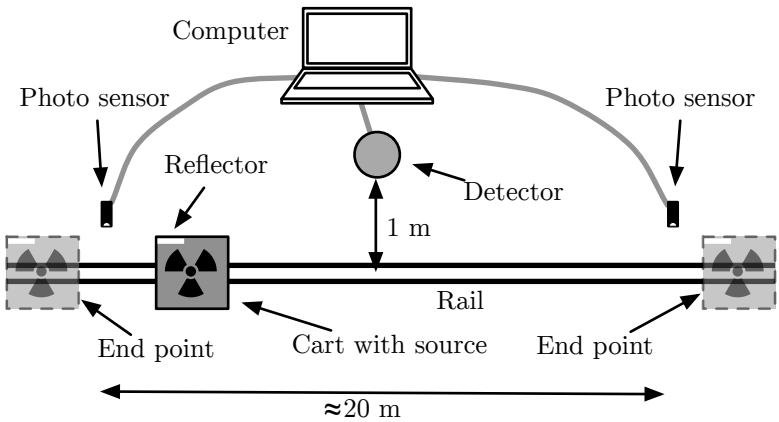

Figure 3.7: The measurement set-up used when testing the mathematical models and the algorithms used for calculating the probability of detecting a moving radioactive source. Adaptation of a figure shown in Paper V.

were examined in some detail in Paper V. The models developed in that paper were tested using detector system 2 placed 1 m away from a track with a moving cart carrying a radioactive source. At the ends of the track, photo sensors were mounted in order to signal the computer connected to the detector when to start and stop the measurements. The cart had a top speed of 5.0 m/s and it took approximately 5 s for it to move from one end of the track to another including the acceleration and deceleration. The set-up is illustrated in Figure 3.7.

The shape of the curve that describes the instantaneous count rate of the detector was tested by moving a 30 MBq ^{137}Cs past the detector 230 times. These measurements were made using list mode and thus the data could be used to create a curve representing the instantaneous count rate.

This experiment was followed by one where the sensitivity of the detector to a 150 kBq ^{137}Cs source moving past it was compared to the calculated sensitivity. The source passed the detector 250 times and the list mode data was then used to create best case and worst case measurements with an integration time of 1 s.

The final test was done by simulating detector system 2 when placed in a backpack and calculating the minimum detectable activity of a

source at minimum distance of 5 and 15 m as the detector system moves past it. Paper V gives a thorough explanation of the set-ups and simulation as well as measurement parameters used.

3.6 Neutron radiation measurements

The models and algorithms needed to calculate the sensitivity of a detector to a moving source were first discussed in Paper III. This was in order to calculate the sensitivity of detector system 3, clad in PVC, to neutron sources. All in all, 4 different configurations of PVC were used and these were compared to detector system 5 which is a dedicated neutron detector. The detector configurations used can be found in Figure 3.8. Efficiency calibration measurements of the detectors were done separately for all the sources listed in Table 3.2. In order to determine how the efficiency was effected by distance, 3 different distances were tested and the angular response was determined by rotating the detector around its short axis to 0, 45 and 90° as illustrated in Figure 3.9.

Optimisation of the region of interest, as described in Section 2.2.3, was also done for the neutron measurements. A through description of this process as well as the efficiency calibration of the detectors can be found in Paper III.

3.7 Scanning detector system

A directional detector was created by placing a cylindrical slit opening collimator over detector system 1. The collimator can be rotated using a computer controlled electric motor, which makes it possible to use the system to scan for radioactive sources over a range of angles. A GPS was used to determine the position of the system, as this information is required by the image reconstruction algorithm described in Section 2.4. An overview of the system is given in Figure 3.10 and Figure 3.11 shows an image of the system when assembled.

In order to determine the angular resolution of the system, a single ^{137}Cs source with an activity of 2 GBq was scanned. The angular resolution was also tested by scanning two 330 MBq sources at 4 different angular separations and determining at which angle the two sources could be distinguished from each other.

In the third test, the image reconstruction capabilities of the system were tested by scanning three ^{137}Cs sources from 4 locations. The three

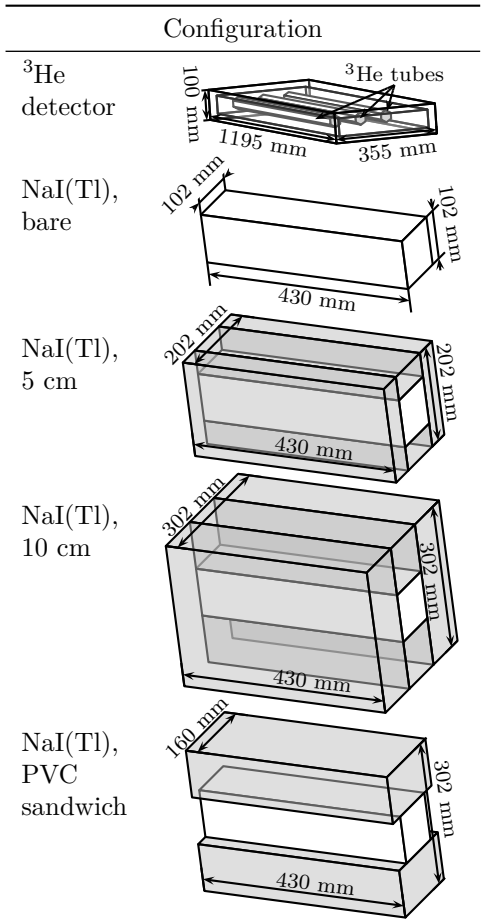

Figure 3.8: The detectors and configurations used when testing the possibility of using NaI(Tl) for detecting neutrons. White shading indicates the detector and the grey transparent volumes illustrates PVC plastic blocks. Based on dimensions given in Paper III.

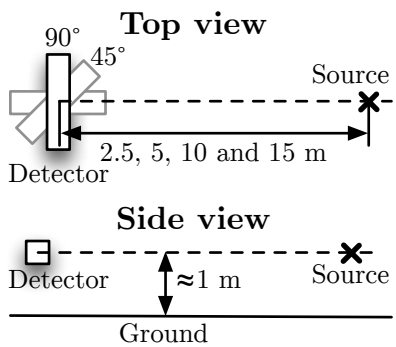

Figure 3.9: Experimental set-up of the detectors used in the testing of detector system 4 as a neutron detectors. Adaptation of a figure shown in Paper III.

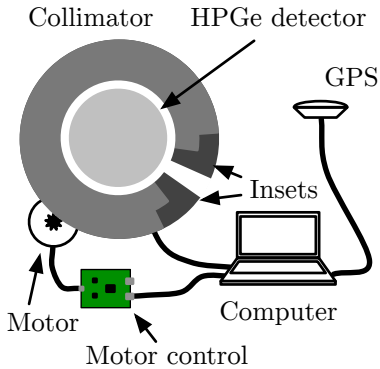

Figure 3.10: Overview of the subsystems of the collimator-based gamma radiation mapping system. Adaptation of a figure shown in Paper IV.

Figure 3.11: The collimator system as used in the tests. The GPS antenna is placed on top of the collimator. The slit opening, showing the HPGe detector, points towards the camera. The stand supports the detector and the rotation mechanism that in turn holds the collimator. The liquid nitrogen Dewar for the HPGe detector can be seen in the middle of the stand. The electronics are outside the field of view of the camera.

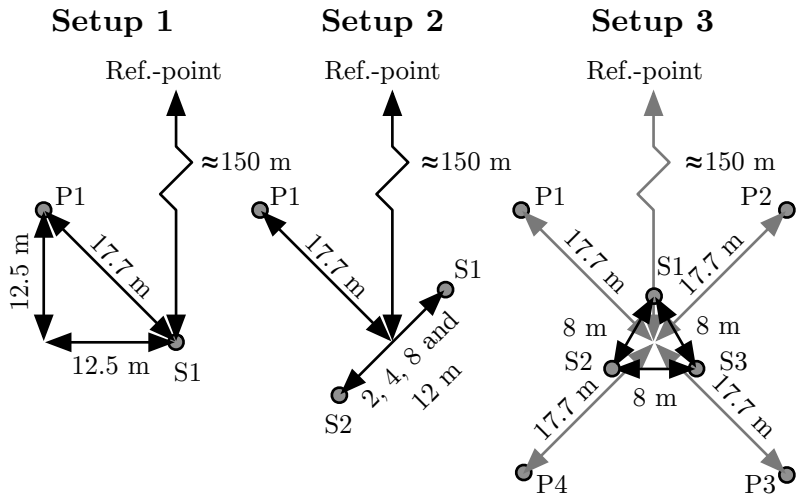

Figure 3.12: Source and detector set-up locations in the tests of the scanning detector system. Points P1 to P4 indicate measurement locations and points S1 to S3 indicate source locations. Adaptation of a figure shown in Paper IV.

set-ups are illustrated in Figure 3.12. The data from these measurements was used as input in the image reconstruction algorithm.

In order to improve the resolution of the system, the data from the second and third test was deconvoluted using the peak from the first experiment as the point spread function (PSF). The deconvoluted data was used to re-calculate the angular resolution and as input to the image reconstruction algorithm.

Chapter 4

Results and discussion

4.1 The deviation display

Three methods of visualising time dependent spectrometric data (explained in Section 2.2.1), the classical waterfall plot, the deviation display, and the modified deviation display were compared (Paper I and Paper II). One of the comparisons, using data from the measurement of a ^{137}Cs source, is shown in Figure 4.1.

When comparing the waterfall plot and the deviation display, the bands representing background radiation seen in the first plot is gone in the deviation display. This makes it possible to clearly distinguish the ^{137}Cs source as seen at approximately 25 s. Also noticeable is the high amplitude noise seen in the high energy range of the deviation display which makes the actual signal of interest less clear. This is caused by the use of the normal distribution to model the background count rate which has the effect of overemphasising the pulses in areas where the pulse rate is low (i.e. above 1500 keV).

The comparison between the original deviation display and the modification of the deviation display (presented in Paper II), shows that the latter reduces the problem of the noise in the high energy region. As the amplitude of the noise has now been reduced, the signal produced by the radioactive source is now easier to see though the noise in the high energy region can still be discerned.

When creating the deviation display, the normal distribution was used to model the background count rate and this was done for several reasons. Doing this is computationally relatively simple and as normal distributions can have different widths they can better model a varying

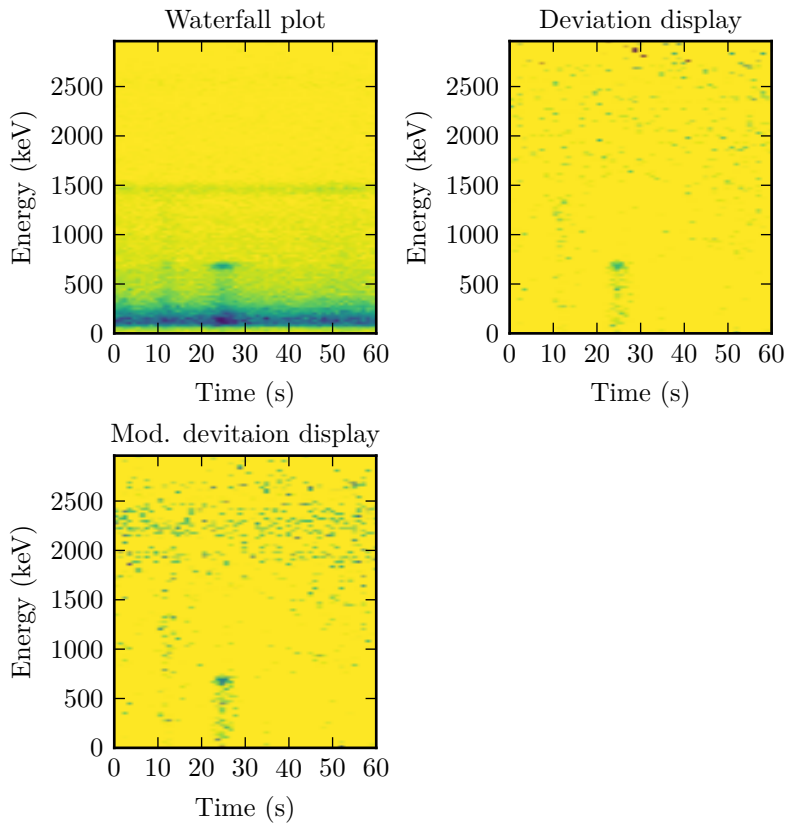

Figure 4.1: The plots illustrates the use of the waterfall plot, deviation display and modified deviation display in that order. The data used to produce the plots is from the measurement of a ^{137}Cs source as it is passed by a moving detector system. The ^{137}Cs source is at its closest point to the detector at ≈ 25 s. Note also the amount of noise found in the deviation display above 1500 keV.

background caused by, for example, bridges, houses or roads with varying amounts of naturally occurring radioactive materials in them. The modification to the algorithm presented in Paper II replaced the normal distribution, for regions where the background is low, with a linear relationship between output value and counts in the background. Due to the low count rate, it is probable that using the Poisson distribution to model this region could improve the visualisation but this was not done due to the higher computational cost of doing so. A possible future development of the deviation display is to, based on background measurements, determine a statistical distribution that better describes the background count rate for different parts of the spectrum and to take advantage of the constantly improving processing power of computers when rendering the display.

Paper I also shows the results of using the deviation display to visualise data from a HPGe detector and from measurements of ^{241}Am and ^{60}Co sources. Both Paper I and Paper II discusses the effect of background count rate and parameters in the visualisation algorithm on the final result when producing the deviation display.

4.2 Backpack measurements

Backpack survey systems based on detector systems 1, 2 and 4 were compared, by surveying a 20 by 20 m^2 area containing three ^{137}Cs sources. For the analysis, several critical limits (see Section 2.1.3), corresponding to true positive probabilities (or confidence levels) ranging from 50% to 99.9% were used to test the data. The areas of the surveys at which the critical limits for the different confidence levels were exceeded are shown in Figure 4.2. The relative sizes of the areas are also presented in Table 4.1.

The table and figure both show that the HPGe detector had the highest probability of detecting the sources given as the true positive areas are greater in all cases. This was not unexpected as the relative efficiency of that the detector is better than that of the NaI(Tl) detector. Although the efficiency is similar to that of the $LaBr_3$:Ce detector, because of the higher energy resolution and lower background, it should perform better in all cases.

The more interesting comparison is between the NaI(Tl) and $LaBr_3$:Ce detectors as they have an approximately equal sensitivity to ^{137}Cs sources in this set-up. Although the $LaBr_3$:Ce detector has the better energy resolution, its internal radioactivity gives it a higher background count

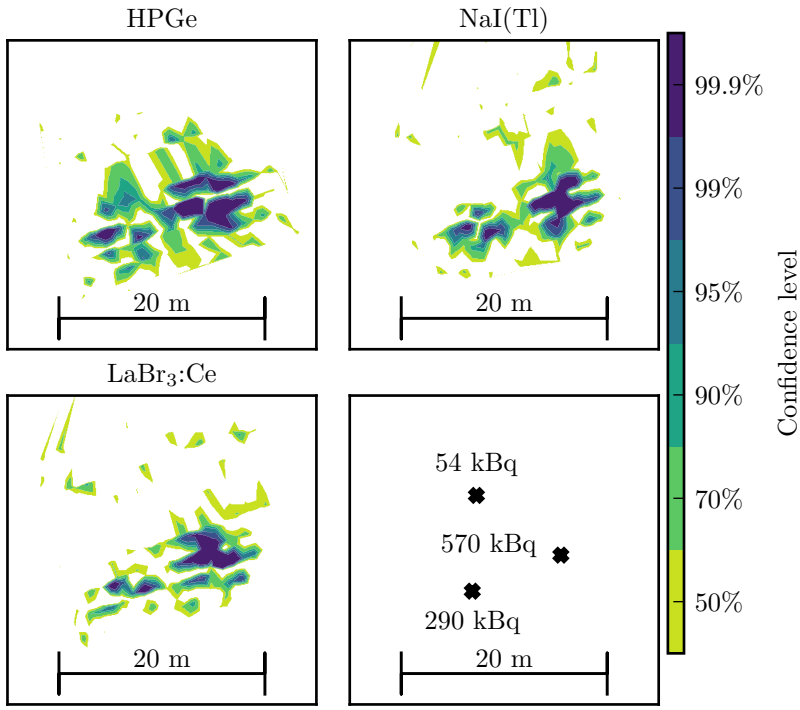

Figure 4.2: The areas in which ^{137}Cs sources were detected with 50–99.9% confidence (true positive probability) when surveyed using a HPGe, NaI(Tl) and $LaBr_3$:Ce detector. Surface areas are given in Table 4.1. Note that the lower right figure illustrate the actual locations and activities of the ^{137}Cs sources. Based on data published in Paper II.

Table 4.1: Percentage of the surveyed area in Figure 4.2 in which ^{137}Cs sources were detected with confidence levels (true positive probability) ranging from 50–99.9%.

Confidence	Detectors		
level	HPGe	$LaBr_3$:Ce	NaI(Tl)
50%	29.9%	23.3%	24.9%
70%	20.4%	15.2%	13.8%
90%	11.5%	7.7%	7.0%
95%	7.4%	5.5%	4.8%
99%	6.1%	3.7%	3.7%
99.9%	4.0%	2.6%	2.6%

rate and this reduces its sensitivity to ^{137}Cs sources. The environment in which these test were done has soil, which is rich in sand, and thus has a relatively low concentrations of naturally occurring radioactive isotopes. It is for this reason expected that the $LaBr_3$:Ce detector should outperform the similar sized NaI(Tl) detector, when searching for ^{137}Cs, in areas where the background count rate is higher than that of the area used in this experiment.

Based on the results of the laboratory tests of the detector systems, the HPGe and $LaBr_3$:Ce detectors were used in the field in a survey of a radioactive waste repository in Georgia. The data collected at this site was analysed with regard to ^{137}Cs. The map produced from these results can be found in Figure 4.3. Based on this map, as well as others discussed in Paper II, several point sources were found outside the repository. The locations of these are noted on the map in Figure 4.4.

The data from the HPGe detector was more useful than the $LaBr_3$:Ce detector in detecting the sources found at the site in Georgia. However, its weight and liquid nitrogen requirement is problematic if used in more extensive surveys.

4.3 Moving detectors

Section 2.2 describes the instantaneous count rate in a detector as it passes a radioactive source. This model was tested using the method explained in Section 3.5 and the result of that experiment is shown in

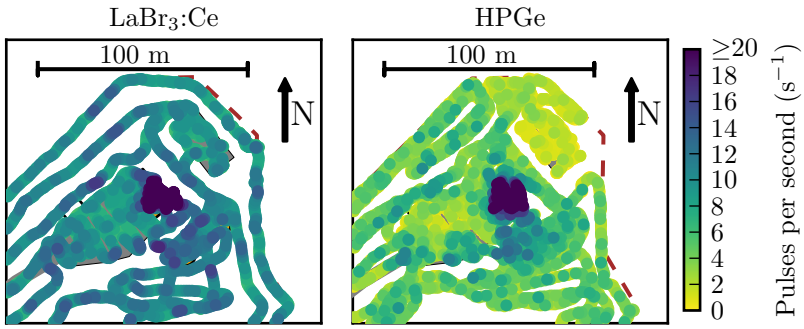

Figure 4.3: Total number of pulses in the ^{137}Cs region of interest when surveying a radioactive waste repository using the HPGe detector and the LaBr3:Ce detector. Due to the high pulse rate directly above the repository, the colour scale is limited to a maximum of 20 counts per second. Based on data published in Paper II.

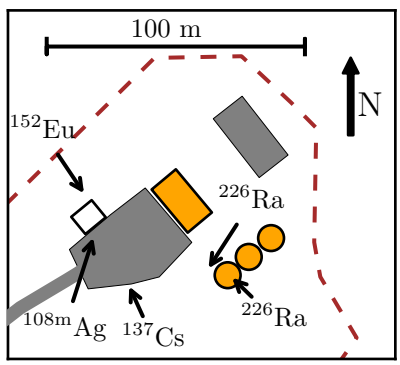

Figure 4.4: The locations of the radioactive sources located outside the radioactive waste repository surveyed in Georgia. The location of the waste repository in the map is marked in Figure 3.6. Adaptation of a figure published in Paper II.

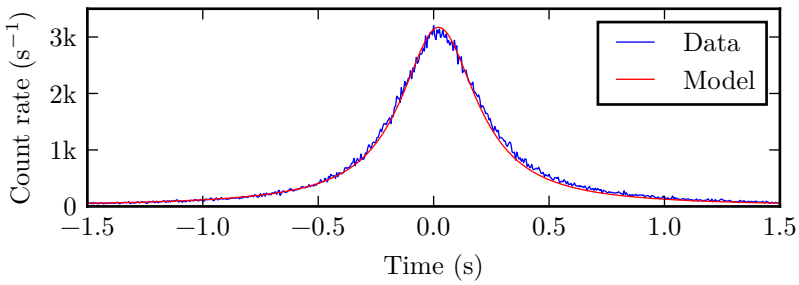

Figure 4.5: Modelled and measured instantaneous count rate from a moving radioactive source. Uncertainties in the measured data are on the order of 0.02 s. Adaptation of a figure shown in Paper V.

Figure 4.5. The figure also include the result of the mathematical model, with the peak height adjusted to fit the data.

It was found that the time it took the cart to move 4.5 m past the detector varied by up to 0.05 s and thus the slight widening seen in the figure was expected. Taking this into account, the data can be considered to be in agreement with the model.

The models used to predict the sensitivity of the detector were tested using a 150 kBq ^{137}Cs source and the results from those experiments are found in Table 4.2. As shown in the table and as expected from the simulations, the worst case scenario had the lowest probability of detecting the source (25% of the passes) whereas the detector can be considered to have detected the source in almost 50% of the passes when operating in list mode. Interestingly, although the detection percentage falls within the uncertainty of the calculations, the worst case scenario fares somewhat better than expected.

One explanation for the relatively large difference between simulated and tested worst case scenario is that the results simply fall within the calculated uncertainty. However, the difference can potentially be caused by the fact that the cart was still accelerating when passing the first photo sensor and thus had a slightly lower velocity than 5.0 m/s when the worst case measurement started. The conclusion drawn from this experiment is that the models used to calculate the sensitivity of a mobile gamma spectrometry system searching for point sources can be considered to be useful.

As a final test, the sensitivity of the detectors when used in a backpack system was calculated for two different minimum source to detector

	Data (%)	Model (%)
Best case	37 ± 4	37 ± 11
Worst case	25 ± 3	16 ± 6
List mode	49 ± 4	43 ± 11

Table 4.2: Measured detection percentage and calculated detection probability of a 150 kBq ^{137}Cs source moving past a detector at a minimum distance of 1 m and a velocity of 5.0 m/s with $\delta = 1$s. The uncertainties in the measured values are due to statistics and the uncertainties in the calculated values are due to the uncertainty in the efficiency measurement. The background count rate was 4.0 per second.

$d_{\mathrm{sr}} = 5$ m		
Calc type	Int. time (s)	Min. act (MBq)
Best	15	2.1
Worst	7.7	2.5
List	15	2.0

$d_{\mathrm{sr}} = 15$ m		
Calc type	Int. time (s)	Min. act (MBq)
Best	46	9.6
Worst	24	11
List	48	9.4

Table 4.3: Minimum detectable activities with optimal integration times when using a ∅7.6 by 7.6 cm^3 NaI(Tl) detector to search for ^{137}Cs sources. The calculations used a false positive rate of 1 per hour, false negative probability of 5%, a background of 20 cps and a speed of 1.2 m/s (walking pace).

distances (5 and 15 m) and integration times from 1–60 s. The results from these calculations, with stars indicating the optimal integration time and minimum detectable activity, are shown in Figure 4.6. The numerical values represented by the stars in the figure can be found in Table 4.3.

The interpretation of Figure 4.6 is similar to that of Figure 2.16 in Section 2.2.4 with the difference in that only the minimum values are shown here which means that the characteristic saw-tooth pattern can not be seen. In the figure, list mode measurements have highest sen-

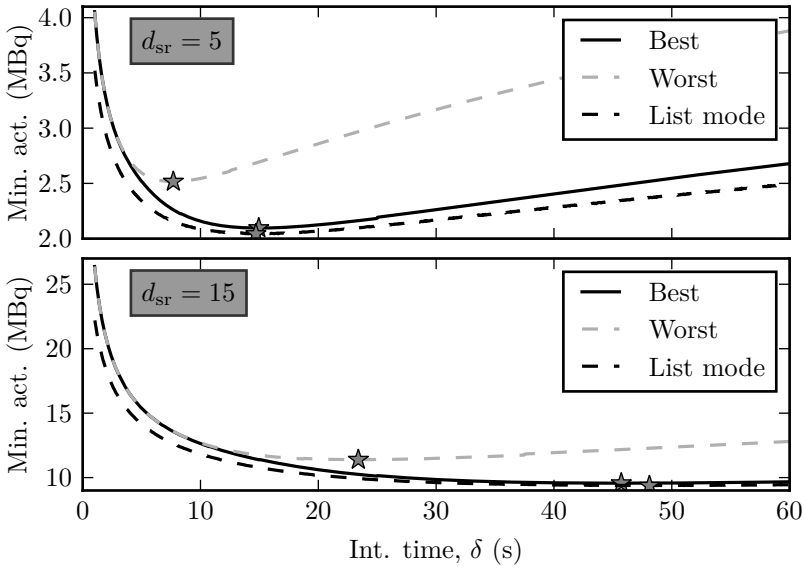

Figure 4.6: Minimum detectable activity as a function of integration time for three measurement scenarios. The figure is based on calculations on a backpack system using a ∅7.6 by 7.6 cm^3 NaI(Tl) detector moving at 1.2 m/s (walking pace), having a false positive rate of 1 per hour, a false negative probability of 5%, a background count rate of 20 cps and measuring a ^{137}Cs source. The stars indicate the optimal integration times. Adaptation of a figure shown in Paper V.

sitivity whereas the worst case scenario results in the worst sensitivity. The small difference between the best case scenario and list mode might lead to the conclusion that list mode measurements are not necessary. Instead, the correct interpretation is that when surveying for radioactive sources, it is not possible to guarantee that a best case scenario is achieved. In practice the results will fall somewhere in between the best case and worst case scenario whereas list mode measurements will always result in better than best case sensitivity.

Existing papers on mobile gamma spectrometry that discusses integration times can be split into two groups, those that suggests integration times of ~ 1 s [10–14] which provides a good spatial resolution of the measurements and those that suggests integration times of 5–10 s [15–17] in order to improve the sensitivity of the system. If the location

of a radioactive source is unknown it is more likely that it is further away from a system used to search for it and thus, based on Figure 4.6, using longer integration times than 10 s is likely to improve the sensitivity of the system. The figure also indicates that picking an integration time that is "too long" is likely to result in a higher probability of detecting the source than an integration time that is "too short". Furthermore, although a long integration time will result in poor spatial resolution of the measurements in mobile gamma spectrometry systems using non-overlapping integrations, using list mode measurements results in a consistently high sensitivity and no loss in spatial resolution.

Many, especially older, mobile gamma spectrometry systems do not have the ability to perform list mode measurements but a sensitivity higher than best case should be possible. By setting the system to use a integration time that is as short as possible and then creating a moving average over a number of these integrations periods, the number of which is decided by the optimal integration time, the sensitivity should approach that of list mode measurements.

Although this research has been focused on the improvement of the probability of detection of a radioactive sources when using an automatic alarm method, the methods used for doing so have wider applications. By using an integration time that is more appropriate for a given measurement scenario, the deviation displays and maps created for visual analysis by humans should improve the probability of detecting a radioactive source. The mathematics that are used to model the instantaneous count rate in a detector can potentially be used to determine the distance between the source and the detector, and by having another detector system that determines which side of the detector that the source is located, the approximate position of the source could then be determined.

4.4 Neutron radiation measurements

In order to maximise the sensitivity of a NaI(Tl) based neutron detector (see Section 2.3), the region of interest of the spectra collected by the detector had to be optimised (as described in Section 2.2.3). The optimisation of region of interest resulted in Figure 4.7. In the left panel of the figure, the upper limit of the ROI was set to 10.5 MeV and thus the figure shows the probability of detecting a neutron source as a function of the lower limit of the ROI. The peak found at 2.8 MeV indicates that this should be the lower limit of the ROI. This is not unexpected as the

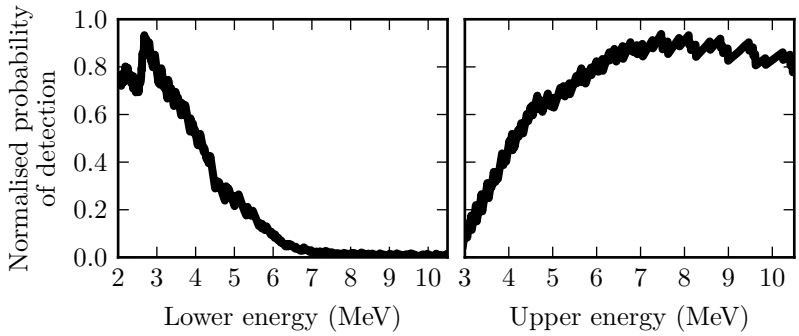

Figure 4.7: These plots were used to determine the optimal energy range (ROI) to integrate over when using a gamma spectrometer as a neutron detector. The left hand panel illustrates that the highest probability of detecting a neutron source is with a lower energy limit of 2.8 MeV and the right hand panel illustrates that upper energy limit should be ~ 8 MeV. Based on data published in Paper III.

highest gamma energy from naturally occurring radioactive materials that can be easily detected is 2.6 MeV.

In the left hand panel of Figure 4.7, the effect on sensitivity when fixing the lower energy limit of the ROI to 2.8 MeV and moving the upper energy limit from 3–10.5 MeV is shown. The sensitivity increases first and then levels out at ~ 7 MeV and appears to decrease at ~ 8 MeV. The background radiation in this part of the energy spectrum originates primarily from cosmic background radiation in the form of muons. As the amount of cosmic background radiation is relatively flat at these energies [57], the decrease at 8 MeV is primarily caused by a decrease in high energy gamma radiation caused by the neutron radiation.

The conclusion from the ROI optimisations is that using the counts in an energy range from 2.8–8 MeV is appropriate when using a NaI(Tl) detector as a neutron detector. It should however be noted that these are approximate values as the figures are based on the mean spectrum from measurement of all three types of neutron sources. For example, the mean energy of the gamma radiation from a ^{252}Cf/^{250}Cf source is lower than that of the other two tested neutron sources.

Using an appropriate region of interest can (as illustrated by the figures) affect the sensitivity of the detector system. Picking an optimised ROI based on the current background count rate and other nuclides

found in the spectrum could potentially improve the sensitivity of the detector system. To the authors knowledge, this is not a question that has been examined in a mobile gamma spectrometry context.

As the mathematical models for calculating the sensitivity of mobile detectors were not fully developed for Paper III, calculations were only done for best, worst and mean case scenarios. The full results for all detector configurations, distances and neutron sources can be found in Paper III. A subset of those results are shown in Figure 4.8 using only the best case scenario in the form of minimum detectable neutron emission rate as a function of minimum source to detector distance.

The configuration with the NaI(Tl) detector covered in 10 cm PVC performed the best overall as only the ^{3}He detector outperformed it in the case of the ^{252}Cf/^{250}Cf source. The reason for the better performance of the ^{3}He detector in case of the ^{252}Cf/^{250}Cf source is likely partially due to the lower energy of the neutrons emitted by the source. The ^{3}He detector should be affected less than the NaI(Tl) based detector by a lower neutron energy. This effect can also be seen in the plots representing the ^{241}AmBe and ^{238}Pu$-^{13}$C sources as the relative difference in sensitivity between the ^{3}He detector and the NaI(Tl) detector covered in 10 cm PVC decreases as the distance increases (i.e the neutrons loose energy).

The gamma radiation emitted directly by the neutron sources is an important factor in detecting neutron sources using a NaI(Tl) detector. As the amount of high energy (> 3 MeV) gamma radiation emitted by ^{241}AmBe sources is greater than ^{252}Cf/^{250}Cf sources for a given neutron emission rate, a NaI(Tl) based neutron detector can have a higher sensitivity to neutron sources than a similar sized dedicated neutron detector. It is likely that if the source is shielded (reducing the amount of direct gamma radiation) or at larger distances (reducing the mean neutron energy), the ^{3}He detector would have a higher sensitivity to neutron radiation. However, whereas ^{3}He based neutron detectors are expensive and rare, it would in comparison be relatively simple to obtain and combine several PVC covered NaI(Tl) detectors in order to create a superior neutron detector which could be used to survey for regular gamma radiation sources at the same time.

4.5 Scanning detector system

The angular resolution as well as the detector response function (see Section 2.4) of the scanning detector system were first investigated. The

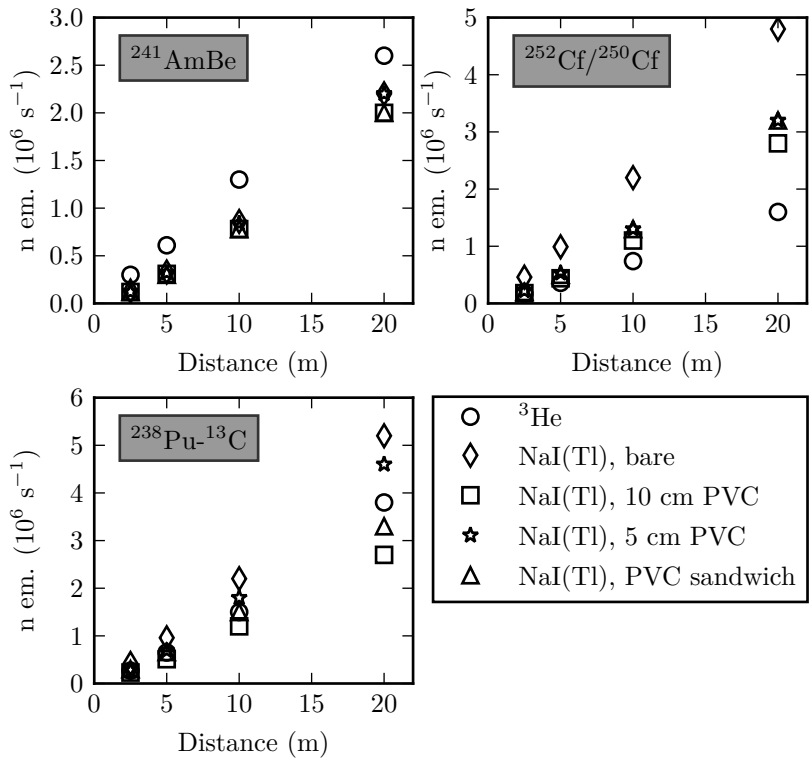

Figure 4.8: The calculated minimum detectable neutron emission rates for three types of neutron sources and 5 different detector configurations at various minimum source to detector distances. The calculations are the best case alignments of the integration periods with a detector speed of 8.3 m/s (30 km/h), a false positive rate of 1 per hour and a false negative probability of 0.05 (5%). Complementary data, including optimal integration times, are given in Paper III.

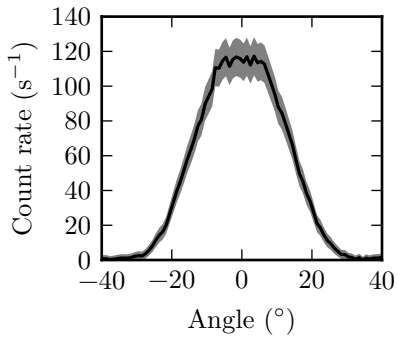

Figure 4.9: The detector response function of using the collimator system to scan over a single ^{137}Cs source. The grey area show the uncertainty range of the measurements. Adaptation of a figure shown in Paper IV.

scan of a single ^{137}Cs source, using set-up 1 in Figure 3.12, resulted in Figure 4.9. The full width at half-maximum (FWHM) of the peak yields a resolution of 30° whereas the 10% valley method gives a resolution of 52°. As the detector has a direct un-obtruded view of the source when the collimator opening is pointing towards it, the peak has a flat top. The rounding at the base of the peak is likely caused by small misalignments in the collimator opening.

Using the data in Figure 4.9 as a point spread function (PSF), the results from measurements of 2 sources at different angular separations were deconvoluted, which resulted in Figure 4.10. The FWHM resolution of the peaks in this figure has a mean value of 10°. The 10% valley resolution calculated from the peaks in the figure suggests a resolution of $\sim 10°$ which is expected as the peaks produced by deconvolution are closer in shape to normal distributions. It is expected that using longer measurement times would result in a higher resolution as the result of the deconvolution is very much dependent on the statistical uncertainty in the data.

The data from the scan of the 3 sources was used in the image reconstruction algorithm without any processing and after deconvoluting the angular data. A comparison between the two after 1 and 15 iterations of the reconstruction algorithm is shown in Figure 4.11. The results after the first iteration indicate that more are needed as not much detail can be discerned. The second row illustrates the result of an appropriate number of iterations. In the two images representing image reconstruction of unprocessed angular data, the indicated distribution of ^{137}Cs remains a blob. This is not the case for the deconvoluted data, which shows that after several iterations of the image reconstruction algorithm, the locations of the three sources.

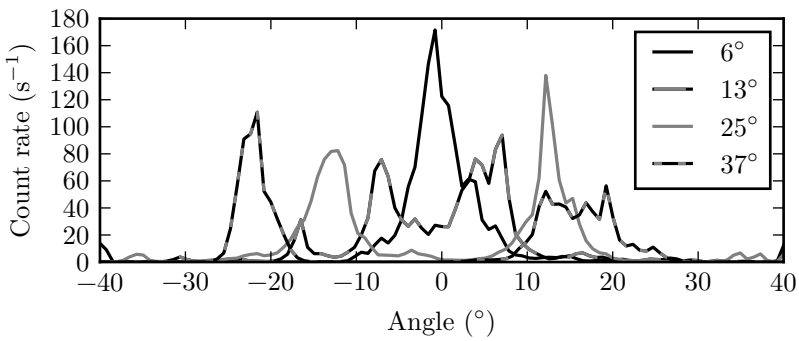

Figure 4.10: The results of scanning two 330 MBq ^{137}Cs sources with four different angular separations and deconvoluting the data. Uncertainties are ≈10%. Adaptation of a figure shown in Paper IV.

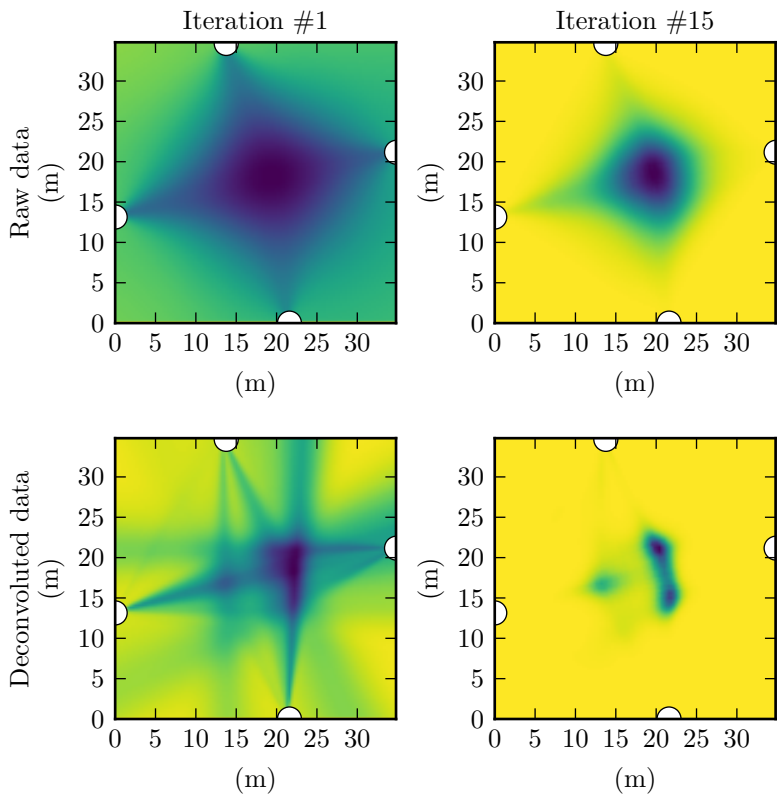

Figure 4.11: The result of the first (left) and the 15th (right) iteration of the image reconstruction algorithm when using unprocessed data (top) and data deconvoluted using an appropriate number of iterations (bottom). The measurements are on set-up 3 (Figure 3.12). The white half-circles indicate the measurement locations. Adaptation of a figure shown in Paper IV.

Chapter 5

Major conclusions

Using Poisson and normal statistics to model the distribution of results in gamma spectrometry measurements is well known yet applying these models in novel ways can improve the probability of detecting a radioactive source. Although the creation of high energy gamma radiation from neutron radiation is well known, its use for neutron radiation detection has received relatively little attention and almost no attention with regard to mobile neutron radiation surveys. Using simple mathematics to model mobile measurements, it is possible to improve the understanding of the statistics of mobile measurements and in turn improve the probability of detecting radioactive sources.

The major conclusion of each paper were as follows:

I. A method for visualising mobile gamma spectrometry data was developed. The new method suppresses the background signal and enhances the dynamic parts of a measurement (from e.g. radioactive point sources). This increases the probability of a radioactive source being detected.

II. The sensitivity of a HPGe, NaI(Tl) and $LaBr_3$:Ce detector when used as backpack systems were tested in a laboratory environment and in the field. As expected, the HPGe detector provided the highest probability of detecting the sources in the tests. The NaI(Tl) and $LaBr_3$:Ce detector proved to have a similar sensitivity in the environments where they were tested.

III. The use of large sized NaI(Tl) detectors covered in PVC as neutron detectors in mobile survey systems was investigated and compared to dedicated ^{3}He based neutron detectors. It was found that the

NaI(Tl) based neutron detectors had a sensitivity comparable to that of large ^{3}He based systems.

IV. A system using a directional gamma spectrometer and an image reconstruction algorithm for mapping radiation fields was developed and tested in a laboratory environment. The system was used to determine the locations of three radioactive sources placed in the survey area.

V. A mathematical model describing the sensitivity of mobile gamma spectrometry systems to point sources was developed and tested. The model was used to develop an algorithm for determining optimal measurement parameters of mobile systems. It was found that choosing parameters based on this algorithm can potentially yield large improvements in the sensitivity of mobile gamma spectrometry systems.

Acknowledgments

Thanks to:

- My supervisors:
  - Christopher Rääf for the scientific advice and for giving me the possibility to have one of the most interesting jobs in the world
  - Robert Finck for sharing your field experience as well as encouraging discussions
  - Sören Mattsson for the enthusiasm and scientific experience
- Co-authors:
  - Karl Östlund for your down to earth attitude and ability to solve practical problems
  - Peder Kock for your knowledge and experience in solving technical problems
  - Christer Samuelsson for your seemingly boundless optimism and willingness to help
  - Joakim Söderberg for having the most interesting waste disposal job in the world
- Colleagues in the environmental radiology group:
  - Jonas, Ünal, Marcus, Mattias, Mats, Kurt, Gertie, Christian, Therése, Maria and Mikael.
- Colleagues in the field of radiation protection in Lund and Malmö:
  - Martin, Hanna, Viveca, Magnus, Cecilia, Daniel, Lars, Peter, Sigrid, David, Mats, Kai *et al.*

- Colleagues in the field of radiation protection and measurement in Sweden and around the world.
- The late Professor Jan Lanke, without whom the mathematics in Paper V would not have been nearly as complete as it is.
- My family and friends, who were willing to listen to me drone on about my research.
- Society, for paying me to do a very interesting and intellectually fulfilling job for 4.5 years.

This research was initated and financed by the Swedish Radiation Safety Authority (SSM) and Lund University in cooperation.

Bibliography

[1] R. F. Mould, *A century of X-rays and radioactivity in medicine: with emphasis on photographic records of the early years*. Bristol, UK: Institute of Physics Publishing, 1993.

[2] H. E. Eskridge, J. E. Hand, and C. A. Willis, "Aerial detection and recovery of a Cobalt-60 source lost in interstate shipment," in *Health Physics Society midyear topical symposium*, (Los Angeles), Gordon and Breach, Science Publishers, Inc., New York, Jan. 1969.

[3] L. J. Deal, J. F. Doyle, P. K. Boyns, and Z. G. Burson, "Locating lost Athena Missile in Mexico by aerial radiological measuring system (ARMS)," *Health Physics*, vol. 23, no. 1, pp. 95–98, 1972.

[4] D. H. Peirson and E. Franklin, "Aerial prospecting for radioactive minerals," *British Journal of Applied Physics*, vol. 2, no. OCT, pp. 281–291, 1951.

[5] United Nations Scientific Committee on the Effects of Atomic Radiation, "Sources and effects of ionizing radiation," tech. rep., New York, Apr. 2011.

[6] International Atomic Anergy Agency (IAEA), "IAEA incident and trafficking database (ITDB)," tech. rep., Vienna, Austria, 2016.

[7] International Atomic Anergy Agency (IAEA), "The radiological accident in Lia, Georgia," tech. rep., Vienna, Austria, Dec. 2014.

[8] J. O. Lubenau and J. G. Yusko, "Radioactive materials in recycled metals," *Health Physics*, vol. 68, pp. 440–451, Apr. 1995.

[9] J. De Laeter, J. Bohlke, P. De Bievre, H. Hidaka, H. Peiser, K. Rosman, and P. Taylor, "Atomic weights of the elements: Review 2000 - (IUPAC technical report)," *Pure Applied Chemistry*, vol. 75, no. 6, pp. 683–800, 2003.

[10] P. Aarnio, J. Ala-Heikkilä, T. Hakulinen, and M. Nikkinen, "Gamma spectrometric monitoring of environmental radioactivity using a mobile equipment," *Journal of Radioanalytical and Nuclear Chemistry*, vol. 233, no. 1-2, pp. 217–223, 1998.

[11] B. D. Geelhood, "Analysis of gamma-ray spectra from an aircraft-mounted array of high-resolution sensors," *Journal of Radioanalytical and Nuclear Chemistry*, vol. 235, no. 1-2, pp. 109–114, 1998.

[12] H. K. Aage and U. Korsbech, "Search for lost or orphan radioactive sources based on NaI gamma spectrometry," *Applied Radiation and Isotopes*, vol. 58, pp. 103–113, 2003.

[13] P. Kock, R. R. Finck, J. Nilsson, K. Östlund, and C. Samuelsson, "A deviation display method for visualising data in mobile gamma-ray spectrometry," *Applied Radiation and Isotopes*, vol. 68, pp. 1832–1838, 2010.

[14] D. M. Pfund, K. K. Anderson, R. S. Detwiler, K. D. Jarman, B. S. McDonald, B. D. Milbrath, M. J. Myjak, N. C. Paradis, S. M. Robinson, and M. L. Woodring, "Improvements in the method of radiation anomaly detection by spectral comparison ratios," *Applied Radiation and Isotopes*, vol. 110, pp. 174–182, Apr. 2016.

[15] R. L. Grasty, "Environmental monitoring by airborne gamma ray spectrometry, experience at the geological survey of Canada," in *IAEA Technical Committee meeting*, (Vienna), pp. 93–101, IAEA, Oct. 1995.

[16] A. N. Tyler, D. C. W. Sanderson, E. M. Scott, and J. D. Allyson, "Accounting for spatial variability and fields of view in environmental gamma ray spectrometry," *Journal of Environmental Radioactivity*, vol. 33, no. 3, pp. 213–235, 1996.

[17] A. J. Cresswell, D. C. W. Sanderson, M. Harrold, B. Kirley, C. Mitchell, and A. Weir, "Demonstration of lightweight gamma spectrometry systems in urban environments," *Journal of Environmental Radioactivity*, vol. 124, pp. 22–28, 2013.

[18] A. J. Cresswell, D. C. W. Sanderson, and D. Maneuski, "Mobile gamma spectrometry measurements of Coneyside Beach, Cumbria," tech. rep., Glasgow, Nov. 2010.

[19] P. Kock and C. Samuelsson, "Comparison of airborne and terrestrial gamma spectrometry measurements - evaluation of three areas in southern Sweden," *Journal of Environmental Radioactivity*, vol. 102, pp. 605–613, 2011.

[20] E. Buchanan, A. J. Cresswell, B. Seitz, and D. C. W. Sanderson, "Operator related attenuation effects in radiometric surveys," *Radiation Measurements*, vol. 86, pp. 24–31, Mar. 2016.

[21] K. Ziock and K. E. Nelson, "Maximum detector sizes required for orphan source detection," *Nuclear Instruments and Methods in Physics Research A*, vol. 579, pp. 357–362, 2007.

[22] S. Billings and J. Hovgaard, "Modeling detector response in airborne gamma-ray spectrometry," *Geophysics*, vol. 64, pp. 1378–1392, Sept. 1999.

[23] H. K. Aage, U. Korsbech, K. Bargholz, S. Bystöm, M. Wedmark, and S. Thorshaug, "Experiences with area specific spectrum stripping of NaI(Tl) gamma spectra," *Radiation protection dosimetry*, vol. 121, pp. 108–121, Dec. 2006.

[24] M. Dowdall, M. Smethurst, R. Watson, A. Mauring, H. Aage, K. Andersson, and S. Pálsson, "Car-borne gamma spectrometry: a virtual exercise in emergency response," *Journal of Environmental Radioactivity*, vol. 107, pp. 68–77, 2012.

[25] P. Kock, C. Rääf, and C. Samuelsson, "On background radiation gradients–the use of airborne surveys when searching for orphan sources using mobile gamma-ray spectrometry," *Journal of Environmental Radioactivity*, vol. 128, pp. 84–90, 2014.

[26] J. A. Kulisek, J. E. Schweppe, S. C. Stave, B. E. Bernacki, D. V. Jordan, T. N. Stewart, C. E. Seifert, and W. J. Kernan, "Real-time airborne gamma-ray background estimation using NASVD with MLE and radiation transport for calibration," *Nuclear Instruments and Methods in Physics Research A*, vol. 784, pp. 287–292, 2015.

[27] A. J. Cresswell, D. C. W. Sanderson, and D. C. White, "^{137}Cs measurement uncertainties and detection limits for airborne gamma spectrometry (AGS) data analysed using a spectral windows method," *Applied Radiation and Isotopes*, vol. 64, pp. 247–253, 2006.

[28] T. Hjerpe and C. Samuelsson, "Shielded and unshielded geometries in the search for orphan sources," *Applied Radiation and Isotopes*, vol. 64, pp. 551–555, May 2006.

[29] A. J. Cresswell and D. C. W. Sanderson, "The use of difference spectra with a filtered rolling average background in mobile gamma spectrometry measurements," *Nuclear Instruments and Methods in Physics Research A*, vol. 607, pp. 685–694, 2009.

[30] L. Wilkinson and M. Friendly, "The history of the cluster heat map," *The American Statistician*, vol. 63, pp. 179–184, May 2009.

[31] E. Lepel, B. Geelhood, W. Hensley, and W. M. Quam, "A field-deployable, aircraft-mounted sensor for the environmental survey of radionuclides," *Journal of Radioanalytical and Nuclear Chemistry*, vol. 233, no. 1-2, pp. 211–215, 1998.

[32] S. Long and L. Martin, "Optimisation of systems to locate discrete gamma-ray sources within a large search area," *Journal of Environmental Radioactivity*, vol. 94, pp. 41–53, 2007.

[33] D. Reilly, N. Ensslin, H. Smith, Jr, and S. Kreiner, *Passive nondestructive assay of nuclear materials*. United States Regulatory Comission, Los Alamos: Los Alamos National Laboratory, Mar. 1991.

[34] R. T. Kouzes, J. H. Ely, L. E. Erikson, W. J. Kernan, A. T. Lintereur, E. R. Siciliano, D. L. Stephens, D. C. Stromswold, R. M. Van Ginhoven, and M. L. Woodring, "Neutron detection alternatives to ^{3}He for national security applications," *Nuclear Instruments and Methods in Physics Research A*, vol. 623, pp. 1035–1045, Nov. 2010.

[35] R. T. Kouzes, "The ^{3}He supply problem," tech. rep., Richland, W.A., USA, Apr. 2009.

[36] D. A. Shea and D. Morgan, "The helium-3 shortage: supply, demand, and options for congress," tech. rep., Washington, D.C., Dec. 2010.

[37] D. J. Mitchell and C. Brusseau, "Neutron counting and gamma spectroscopy with PVT detectors," Tech. Rep. SAND2011-4361, Albuquerque, N.M., USA, June 2011.

[38] P. Holm, K. Peräjärvi, A. Sihvonen, T. Siiskonen, and H. Toivonen, "Neutron detection with a NaI spectrometer using high-energy photons," *Nuclear Instruments and Methods in Physics Research A*, vol. 697, pp. 59–63, 2013.

[39] G. Pausch, C.-M. Herbach, D. Mitchell, R. Lentering, and J. Stein, "Neutron detection based on capture-gamma sensing and calorimetry," in *SPIE Defense, Security, and Sensing*, SPIE, 2012.

[40] D. J. Mitchell, L. T. Harding, and K. R. Smith, "Neutron detection with gamma-ray spectrometers for border security applications," *IEEE TRANSACTIONS ON NUCLEAR SCIENCE*, vol. 57, pp. 2215–2219, Aug. 2010.

[41] L. A. Shepp and Y. Vardi, "Maximum likelihood reconstruction for emission tomography," *Medical Imaging*, vol. MI-1, pp. 113–122, Oct. 1982.

[42] R. WH, "Bayesian-based iterative method of image restoration," *Journal of the Optical Society of America*, vol. 62, pp. 55–59, Jan. 1972.

[43] L. B. Lucy, "An iterative technique for the rectification of observed distributions," *The astronomical journal*, vol. 79, pp. 745–754, June 1974.

[44] E. de Hoffmann and V. Stroobant, *Mass spectrometry. Principles and Applications*, Chichester: John Wiley & Sons, Apr. 2013.

[45] IEEE Standards Board, "IEEE standard test procedures for germanium gamma-ray detectors." The Institute of Electrical and Electronics Engineers, 1987.

[46] R. Hofstadter, "Alkali halide scintillation counters," *Physical Review*, vol. 74, pp. 100–101, May 1948.

[47] S. Johansson, "Measurements of the energy of beta-and gamma-rays with a scintillation counter," *Nature*, vol. 165, p. 396, Mar. 1950.

[48] G. F. Knoll, *Radiation detection and measurement*. New York, N.Y., USA: John Wiley & Sons, 3rd ed., 1999.

[49] E. V. D. van Loef, P. Dorenbos, C. W. E. van Eijk, K. Krämer, and H. U. Güdel, "High-energy-resolution scintillator: Ce^{3+} activated $LaBr_3$," *Applied Physics Letters*, vol. 79, pp. 1573–1575, Sept. 2001.

[50] R. Nicolini, F. Camera, N. Blasi, S. Brambilla, R. Bassini, C. Boiano, A. Bracco, F. Crespi, O. Wieland, and G. Benzoni, "Investigation of the properties of a 1" × 1" $LaBr_3$: Ce scintillator," *Nuclear Instruments and Methods in Physics Research A*, vol. 582, pp. 554–561, 2007.

[51] W. J. Kernan, "Self-activity in lanthanum halides," *IEEE TRANSACTIONS ON NUCLEAR SCIENCE*, vol. 53, pp. 395–400, Feb. 2006.

[52] J. Nilsson, "Using the $LaBr_3$:Ce scintillation detector for mobile γ-spectrometry," Master's thesis, Lund university, Lund, Sweden, June 2011.

[53] K. W. Geiger and C. K. Hargrove, "Neutron spectrum of an Am^{241}-Be(α,n) source," *Nuclear Physics*, vol. 53, no. 2, pp. 204–208, 1964.

[54] R. C. Martin, J. B. Knauer, and P. A. Balo, "Production, distribution, and applications of Californium-252 neutron sources," *Applied Radiation and Isotopes*, vol. 53, pp. 785–792, 2008.

[55] E. A. Lorch, "Neutron spectra of ^{241}Am/B, ^{241}Am/Be, ^{241}AmF, ^{242}Cm/Be, ^{238}Pu/^{13}C and ^{252}Cf isotopic neutron sources," *International Journal of Applied Radiation and Isotopes*, vol. 24, no. 10, pp. 585–591, 1973.

[56] W. Song-Lin, H. Han-Xiong, R. Xi-Chao, L. Xia, B. Jie, N. Yang-Bo, Z. Qi-Ping, Z. Zu-Ying, and K. Xiang-Zhong, "Measurement of the neutron spectrum of a Pu-C source with a liquid scintillator," *Chinese Physics C*, vol. 33, pp. 378–382, May 2009.

[57] E. Tanaka, S. Itoh, and T. Hiramoto, "Cosmic-ray contribution to the background of NaI scintillation spectrometers," *Japanese Journal of Applied Physics*, 1965.